Applied Energy 260 (2020) 114318

Contents lists available at ScienceDirect

Applied Energy

journal homepage: www.elsevier.com/locate/apenergy

Global sensitivity analysis of solid oxide fuel cells with Bayesian sparse polynomial chaos expansions

Qian Shao[a,*], Enlai Gao[a], Thierry Mara[b,c], Heng Hu[a], Tong Liu[d], Ahmed Makradi[e]

[a] School of Civil Engineering, Wuhan University, 8 South Road of East Lake, Wuchang, 430072 Wuhan, PR China
[b] PIMENT, EA 4518, Université de La Réunion, FST, 15 Avenue René Cassin, 97715 Saint-Denis, Réunion
[c] European Commission, Joint Research Centre, Directorate for Foresight, Modelling, Behavioural Insights and Design for Policy, 21027 Ispra (VA), Italy
[d] School of Power and Mechanical Engineering, Wuhan University, 8 South Road of East Lake, Wuchang, 430072 Wuhan, PR China
[e] Luxembourg Institute of Science and Technology, Esch-sur-Alzette, Luxembourg

HIGHLIGHTS

- A Bayesian approach is used to construct machine-learning models for fuel cells.
- A sensitivity analysis is performed on electrochemical performance of fuel cells.
- Impacts of parameters on cell performance are assessed using Sobol' indices.
- The kinetic parameters of electrochemical reactions show critical influence.

ARTICLE INFO

Keywords:
Solid oxide fuel cell
Electrochemical model
Global sensitivity analysis
Polynomial chaos expansion
Bayesian model evidence

ABSTRACT

Uncertainties that commonly exist in mathematical models prevent accurate predictions of solid oxide fuel cell performances and consequently impede the development and application of solid oxide fuel cell technologies. Assessing the impact of uncertain input parameters on cell performance variability is of utmost importance to the improvement of fuel cell models. To this end, a global sensitivity analysis is performed on the electrochemical model of a fuel cell using the Bayesian sparse polynomial chaos expansion approach. With this approach, machine-learning models are constructed to approximate the input-output relationship of the electrochemical model. The first-order, second-order, and total Sobol' indices are then computed analytically to quantify the individual impact of each parameter, the pairwise interaction between them and the total coupling effects over the entire input parameter space. These sensitivity indices show that the kinetic parameters of the electrochemical reaction, such as the activation energy, pre-exponential coefficients, and the electronic transfer coefficient, are the most sensitive parameters that significantly contribute to the variation of cell output voltage, which indicates the requirement for in-depth investigations of these parameters to enhance the accuracy in fuel cell model predictions. This work uncovers the possibility to apply data science techniques to the field of fuel cells. The results of this study not only demonstrate the effectiveness of the Bayesian approach for performing sensitivity analysis on the electrochemical model of a fuel cell, but also shed light on the rational design and optimization of solid oxide fuel cells.

1. Introduction

Solid oxide fuel cell (SOFC), an electrochemical energy conversion device working under high temperature conditions, has been regarded as an environmentally benign energy source that possesses potential benefits consisting of high reaction kinetics, high efficiency, and fuel flexibility [1]. In recent decades, remarkable progress has been made in theoretical, numerical, and experimental studies of optimization, fabrication, and application of SOFC technologies. However, the wide commercialization of SOFCs still faces critical challenges regarding their reliability, efficiency, life expectancy, and so on.

Mathematical modelling is extensively employed as a low cost and efficient alternative to experimental studies [2]. To date, various numerical simulations have been performed with focus on different aspects of SOFC technologies, for instance, understanding the electrochemical reaction mechanism [3] and the failure mechanism [4],

* Corresponding author.
E-mail address: qian.shao@whu.edu.cn (Q. Shao).

https://doi.org/10.1016/j.apenergy.2019.114318
Received 12 September 2019; Received in revised form 8 November 2019; Accepted 1 December 2019
0306-2619/ © 2019 Elsevier Ltd. All rights reserved.

analysing the potential impact of relevant factors [5], selecting proper materials [6], optimizing microstructures of electrodes [7], predicting temperature distribution [8] and thermal stresses [9], studying mass and heat transport [10], investigating gas flow configurations [11], designing complex geometries [12], and predicting the crack propagation [13] and degradations [14]. However, the predictive accuracy of these numerical simulations remains uncertain due to the existence of uncertainties in mathematical models. Typically, the uncertainties in SOFC models arise from the variations of parameters inherent to materials (e.g., electric conductivities, porosities, etc.), manufacturing tolerances, measurement errors, lack of knowledge about parameters (e.g., electronic transfer coefficient, pre-exponential coefficients, etc.), changes of operating conditions (e.g., temperature, pressure, etc.), among others [15]. Thus, evaluating the quality of input parameters and assessing the impact of uncertainty factors on the model outputs are prerequisites for the improvement of the predictive accuracy in SOFC models. For this purpose, global sensitivity analysis (GSA) is an effective tool that has been widely used in various scientific domains. Saltelli et al. [16] defined GSA as '*the study of how uncertainty in the output of a model can be apportioned to different sources of uncertainty in the model input*'. The potential uses of GSA include, but are not limited to, the identification of key parameters that are responsible for output variability, simplification of models by fixing inconsequential parameters, detection of critical regions in input parameter space, prioritization of additional research to enhance the understanding of the model, and evaluation of the coupling effect between different input parameters [15].

In recent years, sensitivity analysis has been applied to various SOFC models for different purposes. Early studies on sensitivity analysis of SOFC models are mainly based on the one-factor-at-a-time method, where the impact of an input parameter on the model response is assessed by varying it alone while keeping other inputs fixed at their baseline values. Using this method, Chan et al. [17] conducted sensitivity analysis on a polarization model of SOFC to study the effect of cell component thickness on the drop in cell voltage. Campanari et al. [18] discussed how the SOFC overpotentials are affected by the different selections of key model parameters involved in the calculation. Nagel et al. [19] investigated the impact of different parameters (such as activation energy, diffusion coefficient, etc.) on the current density and local temperature distributions based on a finite-volume SOFC model. Nam [20] presented a sensitivity map that described the individual effect of each microstructural parameter on current generation in SOFCs. The problem with the one-factor-at-a-time approach is that it does not assess the possible interaction effect of input parameters. To capture the interaction effect, some studies considered combinations of multiple varying input parameters. Gazzarri et al. [21] varied a combination of 21 input parameters in 30 runs of model simulations to study the sensitivity of degradations in SOFCs. Göll et al. [22] conducted sensitivity analysis on the efficiency of a SOFC system by varying 4 parameters simultaneously using a factorial design. Dhingra and Peppley [23] carried out a paired-variable study to evaluate the interactive impact on the SOFC system performance. With the increase of computing power, a large number of numerical simulations become computationally tractable, hence, Monte Carlo-based methods are used in sensitivity analysis to assess the impact of parameters from a statistical point of view. For instance, Cornu and Wuillemin [24] performed sensitivity analysis on a set of 1500 data extracted from Monte-Carlo simulations to assess the impact of random geometric distortions on the performance and reliability of SOFCs. He et al. [25] investigated the individual and simultaneous effects of 7 varying parameters on SOFC stack performance based on Monte Carlo simulations with large sample sizes on the order of 10^3. Further, they quantified the effects of these parameters by variation and correlation coefficients. Some other studies have also been devoted to the quantitative assessment of parameter sensitivities in SOFC models. For instance, Kapadia and Anderson [26] computed sensitivity derivatives of cell voltage with respect to the material properties using the discrete adjoint method. Pan et al. [27] calculated several different sensitivity indicators to rank the contribution of input parameters in SOFC models and further developed reduced order models for SOFC stacks. Although massive applications of GSA have been conducted in different fields, its application towards SOFCs remains limited and primitive [28]. Therefore, further studies on GSA of SOFCs are important for a comprehensive understanding of the impact of uncertain parameters in SOFC models.

To perform GSA in various scientific domains efficiently, various approaches have been proposed. The most widely used GSA techniques are variance-based methods, screening methods, and spectral methods [29]. Among others, variance-based methods have attracted much attention as they are model-free and well applicable to complex physical models, which can be nonlinear, non-smooth, or high-dimensional [16]. Variance-based methods compute Sobol' indices as sensitivity metrics to quantify the impact of model parameters and their interactions over the entire parameter space. To compute Sobol' indices, two approaches are commonly used, namely Monte Carlo-based methods [30] and metamodelling-based methods [31]. The latter usually requires much lower computational effort than the former [32], making it preferable especially for high-dimensional and computationally expensive models. One of the most popular metamodelling-based methods is the sparse polynomial chaos expansion (SPCE) method, which constructs a surrogate model upon multivariate orthogonal polynomials to approximate the input-output relationship of the original physical model [33]. The Sobol' indices are then computed analytically from the SPCE coefficients with negligible computational effort by applying the Parseval-Plancherel theorem. Thus, the key issue becomes how to construct a *good* SPCE model efficiently. Several methods have been developed to build up SPCE models, for instance, the stepwise regression technique [33], the least angle regression algorithm [34], and the projection method with dimension reduction techniques [35]. Recently, a robust and efficient approach based on Bayesian model averaging was proposed to construct SPCE models, namely the Bayesian sparse polynomial chaos expansion (BSPCE) [36]. Specifically, Kashyap information criterion is used within this approach to filter out unimportant polynomial terms, resulting in a simple and sparse polynomial chaos expansion that avoids overfitting and alleviates the curse of dimensionality. This strategy has been validated on several synthetic mathematical examples [36] and proved effective on some numerical problems [37].

Based on the BSPCE approach, the present study aims to quantitatively assess the impact of each uncertain parameter and its interactions with other parameters on SOFC performance by conducting GSA on a verified SOFC electrochemical model. Through this study, we identify key parameters that have major contributions on the variability of SOFC performance, evaluate the applicability of the electrochemical model, understand the behaviour of the SOFC model with respect to its parameters, discover the interactive effects between parameters, and explore the possibility of applying data science techniques to the field of SOFC technology. The results of this study are expected to provide a useful guideline for the experimental measurement, modelling, design, and optimization, as well as to the application of SOFC technologies.

This paper is organized as follows. In Section 2, the mathematical model of electrochemistry in a SOFC unit is introduced, where the formulations of Ohmic, concentration, and activation overpotentials are presented. Section 3 briefly reviews the BSPCE approach and Sobol' indices that are used to perform GSA. Section 4 is devoted to the validation of the SOFC electrochemical model and the construction of BSPCE models. Section 5 presents the results of GSA on the SOFC model, where the impact of input parameters on SOFC overpotentials and the output voltage is discussed in detail. Finally, as a conclusion, our findings regarding the sensitivity of the model-predicted SOFC performance are summarized in Section 6.

2. SOFC mathematical model

Electrochemical reactions between chemical species and electrodes are the basis of energy conversion within a SOFC unit. Electrochemical reactions can only take place at the interface between an electrode and an electrolyte with the existence of chemical species. Assuming a SOFC unit supplied with hydrogen and air, the reactions that take place at the cathode/electrolyte and anode/electrolyte interfaces are

$$\begin{aligned}&\text{Cathode:}\quad \tfrac{1}{2}O_2 + 2e^- \rightarrow O^{2-}\\ &\text{Anode:}\quad H_2 + O^{2-} \rightarrow H_2O + 2e^-\end{aligned} \tag{1}$$

The Nernst equation is commonly used to describe the ideal electromotive force for the above electrochemical reactions [38], also called the open-circuit potential (OCP):

$$U^{\mathrm{OCP}} = U^0_{\mathrm{H_2}}(T) - \frac{\Re T}{2F}\ln\left(\frac{p_{\mathrm{H_2O,f}}}{p_{\mathrm{H_2,f}}\left(p_{\mathrm{O_2,a}}\right)^{\frac{1}{2}}}\right) \tag{2}$$

where $p_{\mathrm{H_2O,f}}$ and $p_{\mathrm{H_2,f}}$ are the partial pressures of water vapour and hydrogen, respectively, at the fuel inlet, and $p_{\mathrm{O_2,a}}$ is the partial pressure of oxygen at the air inlet. The subscripts f and a denote the fuel and air inlets, respectively. $\Re = 8.314$ J mol^{-1} K^{-1} is the universal gas constant. $F = 96,485$ C mol^{-1} is the Faraday constant. T is the operating temperature of the SOFC. $U^0_{\mathrm{H_2}}(T)$ represents the cell potential at a standard operating condition when the pressure is 1 atm. The value of $U^0_{\mathrm{H_2}}(T)$ depends on the operating temperature and the Gibb's free energy [39]:

$$U^0_{\mathrm{H_2}}(T) = (U^0_{\mathrm{H_2}})_{\mathrm{ref}} + \frac{(\Delta S)_{\mathrm{ref}}}{2F}(T - T_{\mathrm{ref}}) \tag{3}$$

where $(U^0_{H_2})_{\mathrm{ref}}$ and $(\Delta S)_{\mathrm{ref}}$ are the standard cell potential and the change of entropy at a reference temperature T_{ref}, given by:

$$(U^0_{H_2})_{\mathrm{ref}} = \frac{(\Delta H)_{\mathrm{ref}} - T_{\mathrm{ref}}(\Delta S)_{\mathrm{ref}}}{2F} \tag{4}$$

$$(\Delta S)_{\mathrm{ref}} = (S_{\mathrm{H_2O}})_{\mathrm{ref}} - (S_{\mathrm{H_2}})_{\mathrm{ref}} - \frac{1}{2}(S_{\mathrm{O_2}})_{\mathrm{ref}} \tag{5}$$

and $(\Delta H)_{\mathrm{ref}}$ is the change of enthalpy during reactions at the reference temperature. Relevant thermodynamic data in the abovementioned equations are listed in Table 1.

Typically, due to the Ohmic (η_{ohm}), concentration (η_{conc}), and activation (η_{act}) overpotentials generated when a SOFC is in service, the output voltage of a cell unit is lower than the ideal open-circuit potential (U^{OCP}), which is given by:

$$U = U^{\mathrm{OCP}} - (\eta_{\mathrm{ohm}} + \eta_{\mathrm{conc,anode}} + \eta_{\mathrm{conc,cathode}} + \eta_{\mathrm{act,anode}} + \eta_{\mathrm{act,cathode}}) \tag{6}$$

where $\eta_{\mathrm{conc,anode}}$, $\eta_{\mathrm{conc,cathode}}$, $\eta_{\mathrm{act,anode}}$, and $\eta_{\mathrm{act,cathode}}$ represent the anodic and cathodic concentration and activation overpotentials. The mathematical models of these overpotentials are detailed in the following subsections.

2.1. Ohmic overpotential

Ohmic overpotential is caused by the resistance to charge transport in SOFCs. Two major types of charged species are involved in SOFC electrochemical reactions: electrons and ions. During electrons transport through the anode and cathode, and ions through the electrolyte, a voltage loss is expended to accomplish this charge transport process. This voltage loss obeys Ohm's law, and thus it is called the Ohmic overpotential. It is linearly proportional to current density, j, with the expression written as follows [38]:

$$\eta_{\mathrm{ohm}} = jR_{\mathrm{ohm}} \tag{7}$$

where R_{ohm} is the area-normalized resistance, namely the area-specific resistance, which is generally measured from experiment. Considering each layer of a SOFC unit individually, and assuming that the overall area-specific resistance R_{ohm} is a function of thickness and conductivities of cell electrodes and electrolyte, we obtain [38]:

$$R_{\mathrm{ohm}} = \frac{\tau_{\mathrm{an}}}{\sigma_{\mathrm{an}}} + \frac{\tau_{\mathrm{el}}}{\sigma_{\mathrm{el}}} + \frac{\tau_{\mathrm{cat}}}{\sigma_{\mathrm{cat}}} \tag{8}$$

where τ_{an}, τ_{el}, and τ_{cat} represents the thickness of the anode, electrolyte, and cathode, respectively. The parameters σ_{an} and σ_{cat} are the electronic conductivities of anode and cathode, respectively, while σ_{el} stands for the ionic conductivity of the electrolyte. Electronic/ionic conductivity quantifies the ability of a material to accommodate electron/ion charge transport under an electric field. Due to the fundamental difference in the transport of electrons and ions, the ion charge transport in a solid electrolyte tends to be far more difficult than electron charge transport in metals. Thus, the ionic conductivity of an electrolyte is typically several orders of magnitude lower than the electronic conductivity of electrodes for SOFCs. Electrical conductivity is strongly dependent on temperature. Generally, the electrical conductivity decreases with increasing temperature in metals, whereas increases with increasing temperature in semiconductors. In this work, considering the commonly used materials for SOFCs, such as Ni/YSZ as the anode, LSM/YSZ as the cathode and YSZ as the electrolyte, the electronic conductivity of the anode is approximated to be linearly proportional to temperature [40]:

$$\sigma_{\mathrm{an}} = A_{\mathrm{an}}(1 - B_{\mathrm{an}}T) \tag{9}$$

with the coefficients A_{an} and B_{an} fitted from experimental data. Meanwhile, the empirical formula of the Arrhenius type is adopted to approximate the electronic conductivity in the cathode and ionic conductivity in the electrolyte [6]:

$$\sigma_k = \frac{A_k}{T}\exp\left(-\frac{B_k}{\Re T}\right) \tag{10}$$

where A_k and B_k are the pre-exponential factor and activation energy for ionic/electronic conduction, respectively, which can be obtained from experiment.

2.2. Concentration overpotential

Electrochemical reactions can only take place at three-phase boundaries (TPB) in SOFCs, which are typically at the interfaces between electrodes and electrolyte. During reactions, the fuel and oxygen are consumed at TPB, resulting in a species concentration gradient through the SOFC's porous electrodes. To maintain effective reactions, mass transport through the electrodes is essentially important. When mass transport effects hinder the reactions, a concentration overpotential appears. Caused by the resistance to mass transport through porous electrodes, the concentration overpotential for a SOFC using H_2 as fuel can be expressed as follows:

$$\eta_{\mathrm{conc}} = \frac{\Re T}{2F}\ln\left(\frac{p_{\mathrm{H_2O,TPB}}p_{\mathrm{H_2,f}}}{p_{\mathrm{H_2O,f}}p_{\mathrm{H_2,TPB}}}\right) + \frac{\Re T}{4F}\ln\left(\frac{p_{\mathrm{O_2,a}}}{p_{\mathrm{O_2,TPB}}}\right) \tag{11}$$

where p_i is the partial pressure of species i. The first and second terms on the right-hand side of Eq. (11) represent the anodic and cathodic concentration overpotentials $\eta_{\mathrm{conc,anode}}$ and $\eta_{\mathrm{conc,cathode}}$, respectively.

To calculate the partial pressures of H_2, H_2O, and O_2 at TPB,

Table 1
Thermodynamic data for chemical species within the SOFC at temperature of 1023 K [39].

Species	$(\Delta H)_{\mathrm{ref}}$ (J mol^{-1})	$(S_i)_{\mathrm{ref}}$ (J mol^{-1} K^{-1})
H_2	0	166.8831
O_2	0	244.3544
H_2O	− 247956	233.7132

different models for mass transport in porous electrodes have been developed [41]. In this work, we assume that on the anode side, the transport of gaseous H_2 and H_2O follow the pattern of equimolar counter-current one-dimensional diffusion. While on the cathode side, the flux of N_2 is zero, and the transport of O_2 is assumed to be one-dimensional self-diffusion [17]. Based on these assumptions, the relations between the partial pressures of species and the current density are given by [17]:

$$p_{\mathrm{H_2,TPB}} = p_{\mathrm{H_2,f}} - \frac{\Re T \tau_{\mathrm{an}}}{2FD_{\mathrm{eff,an}}} j \tag{12}$$

$$p_{\mathrm{H_2O,TPB}} = p_{\mathrm{H_2O,f}} + \frac{\Re T \tau_{\mathrm{an}}}{2FD_{\mathrm{eff,an}}} j \tag{13}$$

$$p_{\mathrm{O_2,TPB}} = \frac{p_0}{\delta_{\mathrm{O_2}}} - \left(\frac{p_0}{\delta_{\mathrm{O_2}}} - p_{\mathrm{O_2,a}}\right) \exp\left(\frac{\delta_{\mathrm{O_2}} \Re T \tau_{\mathrm{cat}}}{4FD_{\mathrm{eff,cat}} p_0} j\right) \tag{14}$$

where p_0 is the operating pressure in the SOFC, and a standard pressure $p_0 = 1$ atm is assumed in this work. The parameter $\delta_{\mathrm{O_2}}$ is given by $\delta_{\mathrm{O_2}} = D_{\mathrm{knudsen,O_2}}/(D_{\mathrm{knudsen,O_2}} + D_{\mathrm{bulk,O_2-N_2}})$. $D_{\mathrm{eff,an}}$ denotes the average effective diffusivity coefficient for a gas mixture of H_2 and H_2O in the anode, with the expression $D_{\mathrm{eff,an}} = (p_{\mathrm{H_2O}}/p_0) D_{\mathrm{eff,H_2}} + (p_{\mathrm{H_2}}/p_0) D_{\mathrm{eff,H_2O}}$. For the sake of simplicity, when the partial pressure of H_2 does not change critically in the anode, $D_{\mathrm{eff,an}}$ is considered as a constant [17]. $D_{\mathrm{eff,cat}}$ represents the effective diffusivity coefficient for O_2 in the cathode, thus $D_{\mathrm{eff,cat}} = D_{\mathrm{eff,O_2}}$.

The effective diffusivity coefficients $D_{\mathrm{eff,H_2}}$, $D_{\mathrm{eff,H_2O}}$, and $D_{\mathrm{eff,O_2}}$ in porous electrodes depend on both the gaseous molecular diffusivity $D_{\mathrm{molecular}}$ and the pore structures inside the electrodes [42]:

$$D_{\mathrm{eff},i} = \frac{\varepsilon_{\mathrm{p}}}{\tau_{\mathrm{tor}}} D_{\mathrm{molecular},i}, \qquad i \in \{\mathrm{H_2},\ \mathrm{H_2O},\ \mathrm{O_2},\ \mathrm{N_2}\} \tag{15}$$

where ε_{p} is the porosity of the electrodes and τ_{tor} represents the tortuosity, which depends on the pore's tortuous nature and typically varies between 1 and 10 in SOFC electrodes [43]. In porous media, the molecular diffusion of gas is basically governed by two possible events, gas-gas collisions and gas-wall collisions, also known as the bulk diffusion and the Knudsen diffusion, respectively. Generally, the molecular diffusivity, $D_{\mathrm{molecular}}$, is attributed to both bulk diffusivity, D_{bulk}, and Knudsen diffusivity, D_{knudsen}, with the following expression:

$$\frac{1}{D_{\mathrm{molecular},i}} = \frac{1}{D_{\mathrm{bulk},i}} + \frac{1}{D_{\mathrm{knudsen},i}} \tag{16}$$

where the Knudsen diffusivity is dependent on the average pore size of the porous medium (r_{p}), the molecular weight of the gas (M_i), and the operating temperature (T), given by:

$$D_{\mathrm{knudsen},i} = \frac{2}{3} r_{\mathrm{p}} \sqrt{\frac{8\Re T}{\pi M_i}} \tag{17}$$

Whereas the bulk diffusivity can be approximated by Fuller-Schettler-Giddings equation in the case of a gas mixture of A and B [42]:

$$D_{\mathrm{bulk},AB} = \frac{10^{-3} T^{1.75} \left(\frac{1}{M_A} + \frac{1}{M_B}\right)^{\frac{1}{2}}}{p_0 \left[(\sum V_A)^{\frac{1}{3}} + (\sum V_B)^{\frac{1}{3}}\right]^2} \tag{18}$$

where $\sum V_A$ and $\sum V_B$ are the sum of the diffusion volume for component A and B, respectively.

2.3. Activation overpotential

Activation overpotential is a voltage loss that is sacrificed to overcome the activation barrier associated with electrochemical reactions in SOFCs. It reflects the kinetics of electrochemical reactions, which is commonly predicted by the Butler-Volmer equation [44]:

$$j = j_{0,\mathrm{electrode}} \left[\exp\left(\frac{\alpha n_e F}{\Re T} \eta_{\mathrm{act,electrode}}\right) - \exp\left(-\frac{(1-\alpha) n_e F}{\Re T} \eta_{\mathrm{act,electrode}}\right)\right] \tag{19}$$

Here, α is the electronic transfer coefficient and n_e is the number of transferred electrons. The value of α depends on the symmetry of the activation barrier. If the reactions are *symmetric*, $\alpha = 0.5$. Otherwise, in most cases, α ranges from about 0.2 to 0.5 [43], depending on the electrochemical reactions and the choice of catalysts. $j_{0,\mathrm{electrode}}$ represents the exchange current density, which describes the rate of exchange between the reactant and product states at equilibrium. $j_{0,\mathrm{electrode}}$ can be calculated as follows [44]:

$$j_{0,\mathrm{anode}} = \gamma_{\mathrm{an}} \left(\frac{p_{\mathrm{H_2,TPB}}}{p_0}\right) \left(\frac{p_{\mathrm{H_2O,TPB}}}{p_0}\right) \exp\left(-\frac{E_{\mathrm{an}}}{\Re T}\right) \tag{20}$$

$$j_{0,\mathrm{cathode}} = \gamma_{\mathrm{cat}} \left(\frac{p_{\mathrm{O_2,TPB}}}{p_0}\right)^{0.25} \exp\left(-\frac{E_{\mathrm{cat}}}{\Re T}\right) \tag{21}$$

where γ_{an} and γ_{cat} are pre-exponential coefficients for reactions on the anode and cathode side, respectively, and E_{an} and E_{cat} are the corresponding activation energy for reactions on the anode and cathode side, respectively. Although a lot of studies have been conducted to estimate the activation overpotential in SOFCs [43], it remains a challenge to provide exact information of all the parameters in the above model. Therefore, a GSA on the SOFC electrochemical model is necessary to quantify the impact of each uncertain parameter on the performance of SOFCs, so as to further determine the sources of uncertainty in predicting and optimizing the SOFC performance.

3. Global sensitivity analysis

In this work, the BSPCE approach is used to perform GSA on the SOFC electrochemical model. To this end, machine-learning models that represent the input-output relationship of the electrochemical model are constructed in the Bayesian framework. Because only the critical polynomial terms are retained within this approach, problems regarding overfitting can be prevented. Moreover, due to its specific properties, the BSPCE model is particularly efficient in computing variance-based sensitivity indices of different orders for each input parameter, requiring negligible additional computational effort subsequent to its construction [36].

3.1. Bayesian sparse polynomial chaos expansion

Let us assume the uncertain input parameters of the SOFC model are independent. A random vector $\boldsymbol{x} = (x_1, x_2, ..., x_n)$ is used to denote the normalized inputs, which are uniformly distributed over the n-dimensional unit hypercube $\mathbb{K}^n$. Meanwhile, the output of interest in the SOFC model is considered as a scalar, where the standardized form of which is denoted by y (i.e., with mean 0 and variance 1). The case of multiple outputs is treated in the same way as discussed in the sequel. The input-output relationship of the SOFC model can be expressed by the following polynomial chaos expansion [32]:

$$y = \mathcal{M}(\boldsymbol{x}) \equiv \sum_{\boldsymbol{b} \in \mathbb{N}^n} a_{\boldsymbol{b}} \psi_{\boldsymbol{b}}(\boldsymbol{x}), \quad \text{with } \psi_{\boldsymbol{b}}(\boldsymbol{x}) = \psi_{b_1 \ldots b_n}(\boldsymbol{x}) = \prod_{i=1}^{n} \psi_{b_i}(x_i) \tag{22}$$

where $\psi_{\boldsymbol{b}}(\boldsymbol{x})$ is a multidimensional polynomial basis, given by the tensor product of univariate orthonormal shifted-Legendre polynomials. The $a_{\boldsymbol{b}}$'s are the polynomial coefficients, and $\boldsymbol{b} = b_1 \ldots b_n$ ($b_i \in \mathbb{N}$, $1 \leqslant i \leqslant n$) is an n-dimensional index, in which b_i represents the degree of the univariate polynomial $\psi_{b_i}(x_i)$. Thus, the total degree of the term $\psi_{\boldsymbol{b}}(\boldsymbol{x})$ is $|\boldsymbol{b}| \equiv \sum_{i=1}^{n} b_i$.

The key of the problem is to identify the polynomial coefficients based on *observed* input-output data. To render this problem computationally tractable, $|\boldsymbol{b}|$ needs to satisfy the condition $|\boldsymbol{b}| \leqslant d$ so that the

polynomial chaos expansion is truncated and only a finite number of terms are retained up to polynomials of degree d. The total number of unknown coefficients, P, in this truncated polynomial chaos expansion can be calculated from the maximal degree, d, and the number of inputs, n, by $P = (n + d)!/(n!d!)$, where P increases polynomially with n and d.

For high-dimensional or high-degree problems, it is obvious that a large number of unknown coefficients needs to be identified within this polynomial chaos expansion, which may lead to computational issues such as overfitting and curse of dimensionality. To prevent these problems, Bayesian model evidence is used to conduct model selection and construct a sparse representation of the model, namely a Bayesian sparse polynomial chaos expansion, where the Kashyap information criterion is adopted to retain only a small number of polynomial basis functions without sacrificing the accuracy [36]. Moreover, based on the Bayes theorem, a maximum a posteriori estimate of polynomial coefficients are computed and used as the most likely parameter set for the BSPCE, considering not only the fit of the *observed* data, but also the prior information about the coefficients (see [36] for more details). We denote the resulting BSPCE as follows:

$$y \simeq \mathcal{M}_{\mathcal{A}}(\boldsymbol{x}) \equiv \sum_{\boldsymbol{b}\in\mathcal{A}} a_{\boldsymbol{b}}\psi_{\boldsymbol{b}}(\boldsymbol{x}), \quad \mathcal{A} \subseteq \mathcal{A}^{d,n} \text{ and } \mathcal{A}^{d,n} \equiv \{\boldsymbol{b} \in \mathbb{N}^n : |\boldsymbol{b}| \leqslant d\} \tag{23}$$

such that $\mathrm{card}(\mathcal{A}) \ll \mathrm{card}(\mathcal{A}^{d,n})$ (the operator 'card' provides the cardinality of a set).

To assess how well the obtained BSPCE model $\mathcal{M}_{\mathcal{A}}$ fits the *observed* data, y, the coefficient of determination R^2 is calculated by

$$R^2 = 1 - \frac{\sum (y - (\sigma_y \mathcal{M}_{\mathcal{A}}(\boldsymbol{x}) + \bar{y}))^2}{\sum (y - \bar{y})^2} \tag{24}$$

where $\bar{y}$ denotes the mean value of the *observed* data and σ_y denotes the standard deviation. As mentioned above, the BSPCE model $\mathcal{M}_{\mathcal{A}}(\boldsymbol{x})$ predicts the standardized values, $\boldsymbol{y}$, which are then transformed into real space using $\bar{y}$ and σ_y. Note that R^2 ranges from 0 to 1. When R^2 approaches 1, this indicates that the BSPCE model fits the data well, otherwise, the BSPCE model cannot well explain the *observed* data. Besides, when (x, y) is used as the training data set, the resulting R^2 based on the same data set can be too optimistic to be a reliable indicator to evaluate the performance of $\mathcal{M}_{\mathcal{A}}$. Thus, R^2 on a validation data set is often adopted to assess the predictive ability of the BSPCE model.

3.2. Derivation of Sobol' indices

The impact of uncertain input parameters on the electrochemical performance of SOFCs is measured by Sobol' indices. They are variance-based sensitivity metrics, which can be easily derived from the BSPCE model $\mathcal{M}_{\mathcal{A}}$ that casts the input-output relationship onto orthonormal polynomials. By Sobol' decomposition [30], the total variance of y can be derived from the coefficients of $\mathcal{M}_{\mathcal{A}}$ analytically:

$$\mathbb{V} = \sum_{\boldsymbol{b}\in\mathcal{A}\setminus\{\boldsymbol{0}\}} a_{\boldsymbol{b}}^2 \tag{25}$$

The partial variance of y due to the s^{th}-order interaction of the subset of input parameters $\{x_{i_1}, ...,x_{i_s}\}$ is computed as follows:

$$\mathbb{V}_{i_1\ldots i_s} = \sum_{\boldsymbol{b}\in\mathcal{I}_{i_1\ldots i_s}} a_{\boldsymbol{b}}^2 \tag{26}$$

where $\mathcal{I}_{i_1\ldots i_s}$ denotes a subset of multidimensional indices in $\mathcal{A}$ such that

$$\mathcal{I}_{i_1\ldots i_s} = \left\{\boldsymbol{b} \in \mathcal{A}: \begin{array}{ll} b_k > 0, & k \in (i_1,\ldots,i_s) \\ b_k = 0, & k \notin (i_1,\ldots,i_s) \end{array}, \quad \forall\, k = 1,\ldots,n\right\} \tag{27}$$

The Sobol' indices are simply the ratio of partial variances to the total variance of y. For instance, the Sobol' index due to the s^{th}-order interactive effect of the input variables $\{x_{i_1}, ...,x_{i_s}\}$ is estimated as $\mathcal{S}_{i_1\ldots i_s} = \mathbb{V}_{i_1\ldots i_s}/\mathbb{V}$, the value of which is always between 0 and 1. Thus a higher Sobol' index implies that the contribution of the associated parameters to the variance of y is more important. In particular, the first-order, second-order, and total Sobol' indices can be derived from the above equations:

$$\mathcal{S}_i = \frac{\mathbb{V}_i}{\mathbb{V}}, \quad \mathcal{S}_{ij} = \frac{\mathbb{V}_{ij}}{\mathbb{V}}, \quad \mathcal{S}_{Ti} = \sum_{\boldsymbol{b}:b_i>0} \mathcal{S}_{\boldsymbol{b}} \tag{28}$$

The first-order Sobol' index $\mathcal{S}_i$ measures the influence due to the parameter x_i alone, which reflects the marginal effect of x_i that is defined by:

$$\int_{\mathbb{K}^{n-1}} \mathcal{M}_{\mathcal{A}}(\boldsymbol{x})\mathrm{d}\boldsymbol{x}_{\sim i} \simeq a_{\boldsymbol{0}} + \sum_{\boldsymbol{b}\in\mathcal{I}_i} a_{\boldsymbol{b}}\psi_{\boldsymbol{b}}(x_i) \tag{29}$$

In the above expression, $\int_{\mathbb{K}^{n-1}} \mathrm{d}\boldsymbol{x}_{\sim i}$ denotes the integration over all variables except x_i. The second-order Sobol' index, $\mathcal{S}_{ij}$, accounts for the cooperative effect of x_i and x_j. The total Sobol' index, $\mathcal{S}_{Ti}$, summarizes the overall contribution of input parameter, x_i, by taking into account its marginal effect and all its interactive effects. It should be noted that the more $\mathcal{S}_{Ti}$ deviates from $\mathcal{S}_i$, the more preponderant the interaction effects among parameters.

4. Construction of BSPCE models

4.1. Verification of the electrochemical model

This work aims to assess the impact of uncertain parameters on SOFC performance by performing GSA on the SOFC electrochemical model. Following the BSPCE approach, the mathematical model described in Section 2 is used to prepare data for training the BSPCE models. Thus, it is a prerequisite to justify the validity of the model in predicting the electrochemical performance of SOFCs. To this end, the existing experimental data from Huang et al. [45] are used to verify this electrochemical model. In [45], a planar SOFC with straight open pores in the anode is tested at different operating temperatures. The anode substrate of this SOFC is prepared using a phase-inversion tape casting method with a mix of NiO (NOVAMET, Japan) and YSZ (TZ-8Y, Tosoh co., Japan) (volume ratio of 57.3:42.7). The thickness of the anode layer is about 1 mm. The sample is cut into a disc shape of diameter 18 mm. A thin YSZ (TZ-8Y, Tosoh co., Japan) electrolyte layer of about 10 μm thick is applied to the anode substrate using the dipcoating method. The composite cathode is made of a mix of LSM and YSZ with a weight ratio of 50:50. The manufactured SOFC is supplied with pure, humidified (~3% H_2O) hydrogen as fuel in the anode, and stationary air as the oxidant in the cathode. The electrochemical performance of the cell is measured under open circuit conditions with an electrochemical system (Zahner Im6ex electrochemical workstation). The operating conditions and model parameters for this SOFC are listed in Table 2, where some parameters are measured or controlled by experiments, such as operating temperature, fuel composition, thickness of electrodes, and others are obtained empirically from existing literature, such as conductivities of electrodes and electrolyte, tortuosity of electrodes, and activation energy. In particular, as this cell contains a finger-like layer in the anode with pores tens of micrometers in diameter, the average pore radius takes a relatively large value, whereas the tortuosity of electrodes is relatively low (see Table 2). Considering the microstructure of porous electrodes, the effective electronic conductivities of anode and cathode are generally lower than that of the intrinsic materials such that $\sigma_{\text{an}} = \xi_{\text{an}}\sigma_{\text{Ni}}$ and $\sigma_{\text{cat}} = \xi_{\text{cat}}\sigma_{\text{LSM}}$. Here ξ_{an} and ξ_{cat} are reduction factors that are primarily determined by the effective relative density of electrode particles [46]. The computation of these factors are detailed in Supplemental Material. For more details regarding the procedure of preparation and measurement for this SOFC, please refer to the literature [45]. It should be noted that the experimental open circuit potentials are usually lower than theoretical values [47], because problems such as current leakage, gas crossover, and side reactions often exist in real SOFC systems [43]. This potential difference is considered as 'leak

Table 2
Parameters used for SOFC electrochemical model verification.

Operating temperature	$T = 973 - 1073$ K [45]
Operating pressure	$p_0 = 1.0$ atm [45]
Fuel composition	x_{H_2}: $x_{H_2O} = 0.97$: 0.03 [45]
Air composition	x_{O_2}: $x_{N_2} = 0.21$: 0.79 [45]
Anode thickness	$\tau_{an} = 1000.0\ \mu$m [45]
Cathode thickness	$\tau_{cat} = 20.0\ \mu$m [45]
Electrolyte thickness	$\tau_{el} = 10.0\ \mu$m [45]
Electronic conductivity of Ni	$\sigma_{Ni} = 3.27 \times 10^6 - 1065.3T\ \Omega^{-1}\ m^{-1}$ [40]
Electronic conductivity of LSM	$\sigma_{LSM} = \frac{4.2\times10^7}{T}\exp\left(\frac{-1150}{T}\right)\ \Omega^{-1}\ m^{-1}$ [40]
Electrolyte ionic conductivity	$\sigma_{YSZ} = 3.34 \times 10^4 \exp\left(\frac{-10300}{T}\right)\ \Omega^{-1}\ m^{-1}$ [40]
Porosity of electrodes	$\varepsilon_p = 0.6$ [43]
Tortuosity of porous electrodes	$\tau_{tor} = 1.0$ [43]
Average pore radius	$r_p = 20.0\ \mu$m [45]
Anode pre-exponential coefficient	$\gamma_{an} = 3.4 \times 10^9$ A m^{-2} [18]
Cathode pre-exponential coefficient	$\gamma_{cat} = 2.0 \times 10^9$ A m^{-2} [18]
Anode activation energy	$E_{an} = 9.0 \times 10^4$ J mol^{-1} [18]
Cathode activation energy	$E_{cat} = 1.03 \times 10^5$ J mol^{-1} [18]
Electronic transfer coefficient	$\alpha = 0.16$ [43]
Leak overpotential	$\eta_{leak} = 0.13$ V [45]

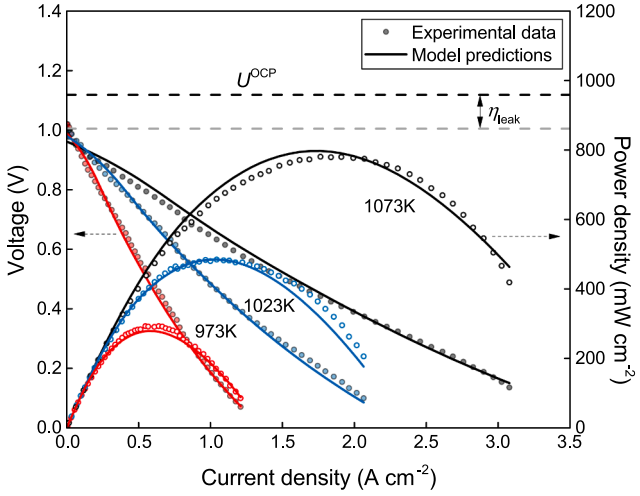

Fig. 1. Comparison of the model-predicted output voltage (the descending curves) and power density (the bell-shaped curves) with the experimental data reported in [45] at different operating temperatures. The black dashed line represents the theoretical open circuit potential at 973 K, and the grey dashed line is the experimental measured open circuit voltage at 973 K. The difference between them approximates the leak overpotential η_{leak}.

overpotential' and kept constant in this study, which yields a cell output voltage such that $U = U^{OCP} - (\eta_{ohm} + \eta_{conc} + \eta_{act} + \eta_{leak})$. Using these parameters, the output voltage and power density ($P = jU$) of the SOFC are computed at different operating temperatures based on the aforementioned electrochemical model. As depicted in Fig. 1, the model-predicted results are compared with the experimental data reported in [45], where a fairly good agreement is found, indicating the validity of the presented mathematical model in predicting the electrochemical performance of SOFCs. To further justify the generality of this electrochemical model, a validation on the experimental data from Ding et al. [48] is performed as well. The related parameters and results are reported in Supplemental Material.

4.2. Definition of input parameters

Before conducting GSA on the electrochemical performance of SOFCs, we need to determine which uncertain input parameters need to be analysed and their possible intervals of variation. Based on the SOFC electrochemical model described in Section 2, 19 uncertain input parameters are defined in Table 3, consisting of parameters related to operating conditions (e.g., operating temperature), geometry of SOFC (e.g., thicknesses of electrodes and electrolyte), microstructure of porous electrodes (e.g., porosity, tortuosity), as well as some empirical coefficients (e.g., electronic conductivity coefficients, pre-exponential coefficients). Uncertainties in some of these parameters, such as electronic conductivity coefficients, tortuosity, and pre-exponential coefficients of electrodes, arise from our imperfect knowledge of the SOFC properties and its electrochemical reactions. While for other parameters, such as operating temperature, anode thickness, etc., the uncertainty is taken into account to study how the variation of these parameters influences the model output. Regarding the varying intervals of these parameters, the temperature is taken to range between 973 K and 1123 K, which is the typical operating temperature of SOFCs [43]. The varying interval of thickness of electrodes and electrolyte are summarized from the review work of Mahato et al. [6]. Herein, a commonly used anode-supported SOFC is considered, with a much thicker anode layer than electrolyte and cathode. The range of values for electronic/ionic conductivity coefficients are determined empirically considering the fitting of experimental data [43,49]. The maximum current density is selected to be 0.8 A cm^{-2} to ensure the predicted output voltage is non-negative. Other parameters are varied in the relatively wide ranges that can be found in literature. For instance, the porosity of electrodes ranges between 0.1 and 0.7 [21], while the pre-exponential coefficients for anode and cathode vary from 2×10^9 to 10^{11} A m^{-2} [18]. Due to lack of prior information, uniform distributions are selected for all parameters to draw general conclusions for the SOFC model. Yet, relatively large intervals are defined to investigate the global effect of model parameters without missing any critical regions. Herein, all parameters are assumed to be statistically independent.

Note that instead of choosing electronic and ionic conductivities (σ_{an}, σ_{act}, and σ_{el}) as uncertain input parameters, the corresponding coefficients (e.g., A_{an}, B_{an}, etc.) are investigated in this work to eliminate the strong dependence of conductivity on the temperature. As it is not easy to measure the coefficients experimentally, the values of A_k and B_k are usually determined empirically. To justify the selected parameter intervals, a group of $2^{11} \times 6$ samples is randomly drawn for the 6 conductivity coefficients from the relevant intervals defined in Table 3. Using these samples, the conductivities σ_{an}, σ_{act}, and σ_{el} are computed by Eqs. (9) and (10), leading to a size of 2^{11} data for each electric conductivity as plotted in Fig. 2. It is observed in Fig. 2 that the ionic conductivity of the electrolyte is orders of magnitude lower than the electronic conductivity of electrodes. This is typical in SOFCs due to the different mechanisms for electronic and ionic conduction, as mentioned earlier. Besides, conductivities of some commonly used electrodes and electrolytes, such as Ni/YSZ, LSM, GDC, etc., are marked in Fig. 2 with red diamonds. It is noted that all these materials' conductivities are reasonably located within the range of Monte Carlo samples, which indicates the justifiability of selected parameters intervals.

4.3. Training and validation of BSPCE models

To perform GSA, machine-learning models are constructed with BSPCE to describe the relationship between the input parameters and the output performance of SOFCs. Hence several output metrics are assessed to quantify the electrochemical performance of SOFCs, including the Ohmic, concentration, and activation overpotentials (η_{ohm}, $\eta_{conc,anode}$, $\eta_{conc,cathode}$, $\eta_{act,anode}$, and $\eta_{act,cathode}$), the cell output voltage (U), the power density (P), as well as the voltage efficiency of the fuel cell ($\varepsilon_{voltage} = U/U^{OCP}$). To train the machine-learning BSPCE models, a data set including information about the input parameters and output metrics is created. For this purpose, an experimental design of size $2^{12} \times 19$ is randomly drawn from the 19 input parameter intervals with quasi-Monte Carlo sampling. Then, the output metrics are computed

Table 3
Uncertain input parameters of the SOFC electrochemical model.

Parameter	Notation	Unit	Type of PDF	Range of values	Reference
Operating temperature	T	K	Uniform	[973, 1123]	[43]
Anode thickness	τ_{an}	m	Uniform	[500, 1000]× 10^{-6}	[6]
Cathode thickness	τ_{cat}	m	Uniform	[10, 100]× 10^{-6}	[6]
Electrolyte thickness	τ_{el}	m	Uniform	[5, 20]× 10^{-6}	[6]
Anode electronic conductivity	A_{an}	Ω^{-1} m^{-1}	Uniform	[2, 3500]× 10^{3}	[49]
coefficients	B_{an}	K^{-1}	Uniform	[3, 7]× 10^{-4}	[49]
Cathode electronic conductivity	A_{cat}	K Ω^{-1} m^{-1}	Uniform	[4, 20]× 10^{7}	[43]
coefficients	B_{cat}	J mol^{-1}	Uniform	[5, 20]× 10^{3}	[43]
Electrolyte ionic conductivity	A_{el}	K Ω^{-1} m^{-1}	Uniform	[3, 30]× 10^{7}	[43]
coefficients	B_{el}	J mol^{-1}	Uniform	[5, 10]× 10^{4}	[43]
Porosity of electrodes	ε_p	/	Uniform	[0.1, 0.7]	[21]
Tortuosity of porous electrodes	τ_{tor}	/	Uniform	[1, 10]	[43]
Average pore radius	r_p	m	Uniform	[0.3, 20]× 10^{-6}	[43,45]
Anode pre-exponential coefficient	γ_{an}	A m^{-2}	Uniform	[2, 100]× 10^{9}	[18]
Cathode pre-exponential coefficient	γ_{cat}	A m^{-2}	Uniform	[2, 100]× 10^{9}	[18]
Anode activation energy	E_{an}	J mol^{-1}	Uniform	[9, 14]× 10^{4}	[18]
Cathode activation energy	E_{cat}	J mol^{-1}	Uniform	[9, 14]× 10^{4}	[18]
Electronic transfer coefficient	α	/	Uniform	[0.15, 1]	[43]
Current density	j	A cm^{-2}	Uniform	[0, 0.8]	

using the SOFC electrochemical model described in Section 2, resulting in a $2^{12} \times 27$ data matrix, which consists of $2^{12} \times 19$ input samples and $2^{12} \times 8$ output metrics. Randomly choosing $2^{11} \times 27$ samples from the data matrix as a training set, 8 machine-learning BSPCE models are constructed, respectively, for the 8 scalar output metrics based on the BSPCE approach.

As shown in Fig. 3, the BSPCE-predicted overpotentials and output voltage are firstly compared with the model-calculated data from the training set, and then tested by a validation set consisting of an extra 2^{11} Monte Carlo simulations. Note that this validation set does not coincide with the training set used for the construction of the BSPCE model. Besides, as the power density and voltage efficiency of the SOFCs are strongly dependent on the current density and cell output voltage, respectively, here we focus on the GSA of overpotentials and output voltage. The results for power density and efficiency are shown in the Supplemental Material. The comparisons in Fig. 3 show that, for Ohmic and concentration overpotentials (η_{ohm}, $\eta_{conc,anode}$, and $\eta_{conc,cathode}$), remarkable agreement is obtained between the model-calculated overpotentials and the BSPCE-predicted values, with the coefficients of determination (R^2) for both training and validation sets being larger than 0.97. Basically, R^2 for the validation set is slightly lower than that of the training set, with a difference of around 0.01. An excellent match is found between the ideal fit and the linear fit of model-calculated data to the BSPCE-predicted values, which confirms that the BSPCE models reproduce well the physical model-calculated Ohmic and concentration overpotentials. Meanwhile, for the activation overpotential ($\eta_{act,anode}$, $\eta_{act,cathode}$), discrepancies between the BSPCE-predicted and model-calculated values are observed. R^2 for the training set is still larger than 0.97, while the validated R^2 decreases to less than 0.97 and 0.94 for the anode and cathode activation overpotential, respectively. The deviation between the ideal fit and the linear fit to BSPCE-predicted values shows a slight underestimation of the BSPCE-predicted values compared to the model-calculated results at high activation overpotentials. Indeed, the input-output relationship is more complex for the activation overpotential than for Ohmic and concentration overpotentials, as presented in Section 2. Moreover, the relevant uncertain parameters' intervals for activation overpotential model are relatively generous, resulting in a large uncertainty in the output data set (ranging from 0 V to about 1.05 V). Therefore, the activation overpotential is more difficult to predict than Ohmic and concentration overpotentials via the machine-learning BSPCE model. Regarding the overall output voltage, Fig. 3 shows that R^2 decreases to 0.95 and 0.92 for the training and validation set, respectively, indicating a discrepancy between the BSPCE-predicted values and the model-calculated data. The linear fit to the BSPCE-predicted values reveals a slight overestimation at low voltages. The output voltage of SOFC is not easy to predict due to the lack of knowledge in SOFC working mechanisms and its complex relations with input parameters. The BSPCE model developed here exhibits a similar issue. Overall, all BSPCE models show good ability to reproduce both the training and validation sets. Thus, the accuracy of these models is sufficient to obtain reliable sensitivity indices.

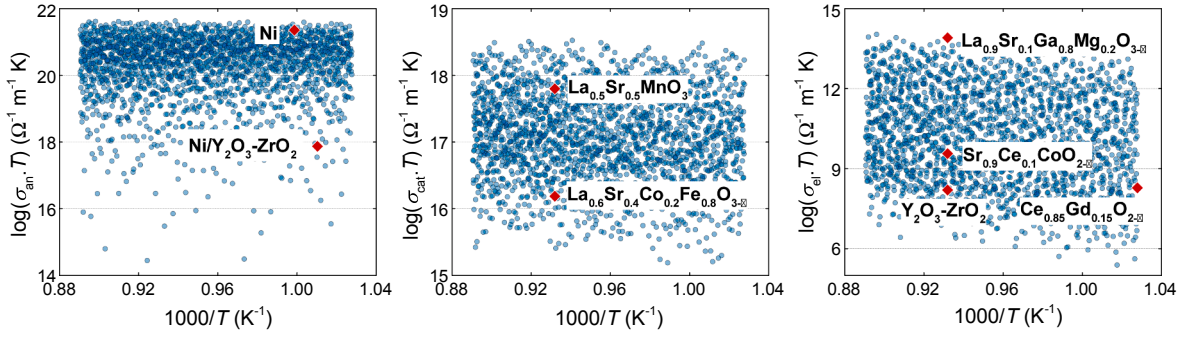

Fig. 2. Electronic and ionic conductivities of the anode, cathode, and electrolyte with respect to temperature variation based on randomly sampled conductivity coefficients. Conductivities of some typical materials used for SOFC anode [49], cathode, and electrolyte [43] are marked with red diamonds, which are well located within the range of sampled conductivities.

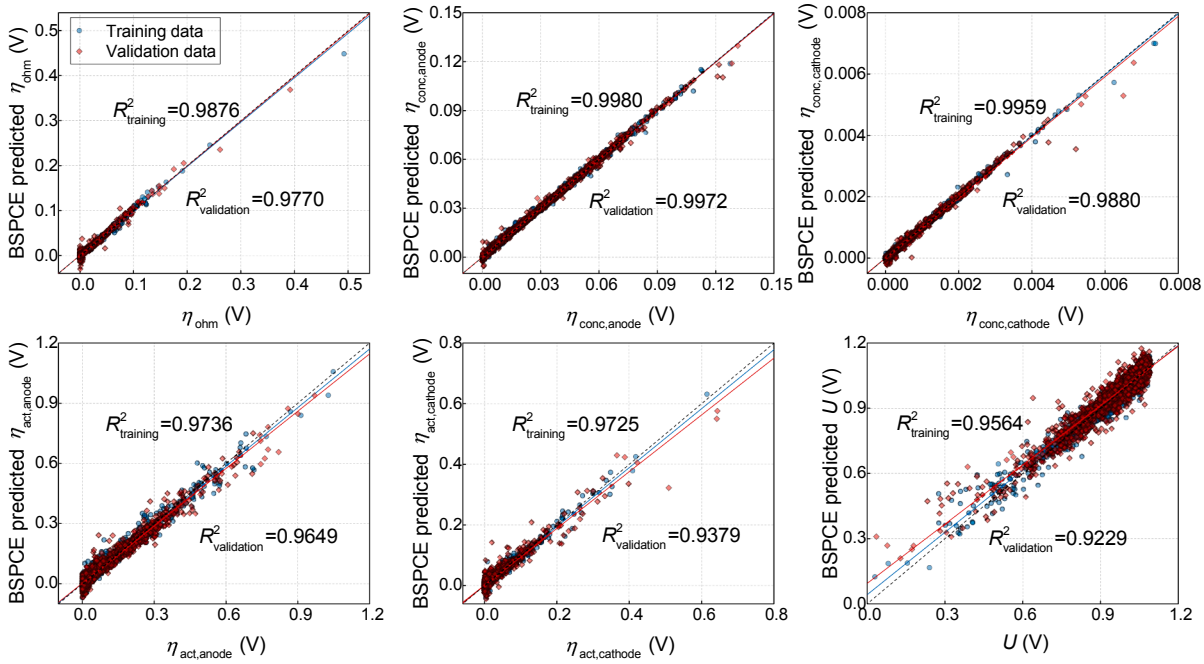

Fig. 3. Comparison of model outputs (η_{ohm}, $\eta_{conc,anode}$, $\eta_{conc,cathode}$, $\eta_{act,anode}$, $\eta_{act,cathode}$, and U) between the BSPCE-predicted values and model-calculated data, including the training set and the validation set. The dashed lines are the ideal 1:1 ratio, whereas the solid lines are the fit to the predicted values. The deviations between the dashed lines and the solid lines show slight underestimation at high values for the activation overpotential, and slight overestimation at low values for the output voltage.

5. Results and discussions

5.1. GSA of overpotentials

The BSPCE models presented in Section 4 are used to perform GSA on the electrochemical performance of a SOFC unit, based on which the first-order and total Sobol' indices are computed analytically for each input parameter. The Sobol' indices of the most sensitive parameters for Ohmic, concentration, and activation overpotentials are shown in Fig. 4. In each panel, the *x*-axis represents the input parameters, and the *y*-axis stands for the values of relevant total and first-order Sobol' indices. The total Sobol' indices, depicted as blue bars in Fig. 4, quantify the contribution of both individual and interactive effects of parameters to the variance of overpotentials; while the first-order indices, presented by red bars, measure merely individual parameter contributions to the variance of model outputs. The distance between the two bars reveals the total interactive contribution of one parameter with all the other parameters. We note in Fig. 4 that the total Sobol' indices are generally higher than the corresponding first-order Sobol' indices, implying the existence of interactive effect among parameters. On one hand, to further study the univariate influence of each parameter onto the model output, the marginal effect of sensitive parameters is plotted in Fig. 5. This univariate effect is computed by considering the evolution of model outputs with respect to a single parameter averaged on other parameters (see Eq. (29)), and then scaled for ease of view. On the other hand, to investigate the interactive effect, the second-order Sobol' indices, which quantify the contribution of pairwise interactions between two parameters on the variance of model outputs, are calculated and plotted using 3D histograms as shown in Fig. 6.

Ohmic overpotential – Examining the Sobol' indices for Ohmic overpotential in Fig. 4 shows 5 sensitive parameters, i.e., the temperature T, the thickness of electrolyte τ_{el}, the ionic conductivity coefficients of electrolyte A_{el} and B_{el}, and the current density j. Among these parameters, A_{el} and B_{el} are the most sensitive ones, accounting for about 40% of the total variance in the Ohmic overpotential, which indicates that the ionic conductivity of the electrolyte plays a rather important role in Ohmic overpotential. Besides, it is noted that the thickness and electronic conductivities related to the anode and cathode have a negligible influence on the Ohmic overpotential. This is typical in SOFCs as the ionic conductivity of the electrolyte is normally several orders of magnitude lower than the electronic conductivities of electrodes, making the ionic charge transport far more difficult than electronic charge transport. Thus, the resistance to ionic transport in electrolytes tends to be the main source for Ohmic overpotential in SOFCs. Besides, it is observed in Fig. 4 that the thickness of the electrolyte τ_{el} has a relatively small impact on Ohmic overpotential. This is due to the relatively small uncertainty range defined for τ_{el} in the case of anode-supported SOFCs. For other types of SOFCs, such as electrolyte-supported SOFCs, the thickness of the electrolyte may show a more significant contribution on Ohmic overpotential.

The marginal effects of parameters displayed in Fig. 5 are found to be consistent with relevant Sobol' indices as shown in Fig. 4. It is observed in Fig. 5 that the Ohmic overpotential decreases with the increase of operating temperature, T. Indeed, the higher temperature enhances the ionic conductivity of electrolyte, which in turn reduces the resistance to charge transport. Conversely, the increase of electrolyte thickness τ_{el} slightly raises the Ohmic overpotential, because a longer path makes it more difficult for ionic charge transport in SOFC electrolytes. The coefficients A_{el} and B_{el} show a significant univariate effect on Ohmic overpotential. In particular, when A_{el} is less than 12×10^7 K Ω^{-1} m^{-1} and B_{el} is larger than 8×10^4 J mol^{-1}, the Ohmic overpotential increases dramatically. Typically, ionic conduction occurs in an electrolyte via the vacancy diffusion mechanism, where the ion mobility is dependent on the rate of the hopping process of ions from position to position within the lattice. This hopping rate is exponentially activated by the size of the energy barrier for motion. In general, materials with a higher activation energy B_{el} yield lower ionic conductivity, and thus higher Ohmic overpotential. Contrarily, as A_{el} reflects the attempt frequency of the hopping process, the increase of A_{el} enhances the ionic conductivity of materials and hence reduces the Ohmic overpotential. The values of A_{el} and B_{el} are related to inherent properties of electrolyte materials, such as the site fraction of oxygen

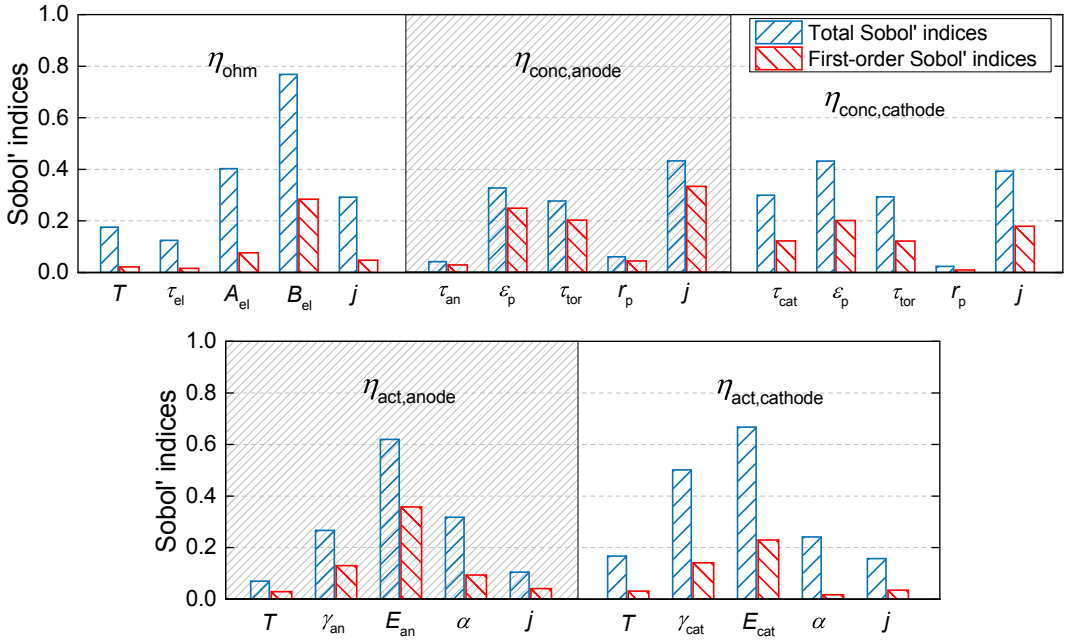

Fig. 4. Total and first-order Sobol' indices of the most sensitive parameters for Ohmic, concentration, and activation overpotentials.

vacancies, the jump distance of an ion, and the entropy and enthalpy of migration. Actually, exact values of these parameters are difficult to obtain either experimentally or theoretically, which eventually leads to large uncertainties in model-predicted Ohmic overpotentials. For instance, it is noted in Fig. 3 that the maximum η_{ohm} reaches more than 0.4 V in the training samples, while the minimum η_{ohm} is about 0 V. Therefore, in order to make precise predictions of Ohmic overpotential in SOFCs, it is important to accurately measure the ionic conductivity of the electrolyte or the corresponding coefficients.

Moreover, it is noted in Fig. 4 that the distance between the total and first-order Sobol' indices are considerably large, indicating that remarkable interactive effect exists among these parameters. As depicted in Fig. 6, for Ohmic overpotential, all 5 sensitive parameters are found to interact with each other, among which the coefficient B_{el} shows the most significant interaction effect with other parameters. For instance, A_{el} and B_{el} presents a highly pairwise interaction effect on Ohmic overpotential, which contributes even more than the individual effect of A_{el}. This suggests that to design a SOFC with low Ohmic overpotential, it is much more efficient to optimize A_{el} and B_{el} simultaneously than the individual adjustment of each parameter. Besides, even though τ_{el} shows slight marginal effect on the Ohmic overpotential, its interaction with B_{el} is significant, implying that the contribution of τ_{el} cannot be neglected in the optimal design of SOFCs. Actually, except for the individual effect of each parameter, the variance of Ohmic overpotential is remarkably attributed to B_{el} interacting with other parameters, i.e., T, τ_{el}, A_{el}, and j. Therefore, all 5 input parameters need to be considered carefully to predict Ohmic overpotential in SOFCs owing to their critical contributions to interaction effects.

Concentration overpotential – First-order and total Sobol' indices of the most sensitive parameters for anodic and cathodic concentration overpotentials are displayed in Fig. 4. Obviously, the porosity ε_p, tortuosity τ_{tor} of electrodes and current density j are the most important parameters, which explain 50%-80% of the total variance in the concentration overpotential. The thickness of cathode, τ_{cat}, shows a higher sensitivity index than the thickness of anode, τ_{an}, indicating that the cathodic concentration overpotential is attributed more to the thickness of the electrode than the anodic concentration overpotential. This may be explained by two reasons, i.e., the relatively larger uncertainty range defined for τ_{cat} as compared to that of τ_{an}, and different assumptions that have been made to model the gas diffusion in the anode and cathode layers. It is also worthwhile noting that, although the temperature is taken into account in the concentration overpotential model, it is found to exhibit a negligible effect on concentration overpotential at the present conditions considered in this work.

Examining the marginal effect in Fig. 5 shows that the concentration overpotential increases with the increase of τ_{an} and τ_{cat}. Apparently, the increase of porous electrode thickness results in thicker diffusion layers, leading to higher concentration losses. The porosity, ε_p, tortuosity, τ_{tor} and average pore radius, r_p, characterize the main features of the microstructure for porous electrodes. High porosity, low tortuosity, and large pore radius would enhance the effective diffusivity of the electrode and make the species diffusion more efficient. Thus, the concentration overpotential can be ideally mitigated by optimizing the microstructure of porous electrodes. For example, Fig. 5 shows a remarkable increase of concentration overpotential when the porosity is less than 0.3, which suggests an optimal design of electrode porosity to be larger than 0.3. Besides, the current density has a significant effect on the concentration overpotential as well. Increasing the current density intensifies the reactant depletion on the electrode/electrolyte interface, and thus enhances the concentration losses.

Checking the total and first-order Sobol' indices of concentration overpotential implies that interactions between parameters are virtually absent in the anodic concentration overpotential model, whereas more interaction effects between parameters are exhibited for the cathodic concentration overpotential. As illustrated in Fig. 6, the current density, j, tortuosity, τ_{tor}, porosity, ε_p, and thickness of cathode, τ_{cat}, show the most significant pairwise interactions on $\eta_{conc,cathode}$. The difference between the sensitivity effects of parameters on $\eta_{conc,anode}$ and $\eta_{conc,cathode}$ is due to the distinct diffusive mechanisms of H_2, H_2O, and O_2 in the anode and cathode, where different theories and models are used to compute the concentration overpotentials. Furthermore, comparing the values of $\eta_{conc,anode}$ and $\eta_{conc,cathode}$ in Fig. 3, we find that $\eta_{conc,anode}$ varies between 0 and 0.15 V, while $\eta_{conc,cathode}$ is less than 0.008 V. Typically, O_2 diffuses more slowly than H_2, and air is often used instead of pure O_2 in SOFCs, leading to more severe concentration overpotential in the cathode. However, this is not the case herein. This is because the anode-supported SOFC considered in this work has a much larger anode thickness than that of cathode, resulting in a longer path of species diffusion in the anode layer. Therefore, to reduce the

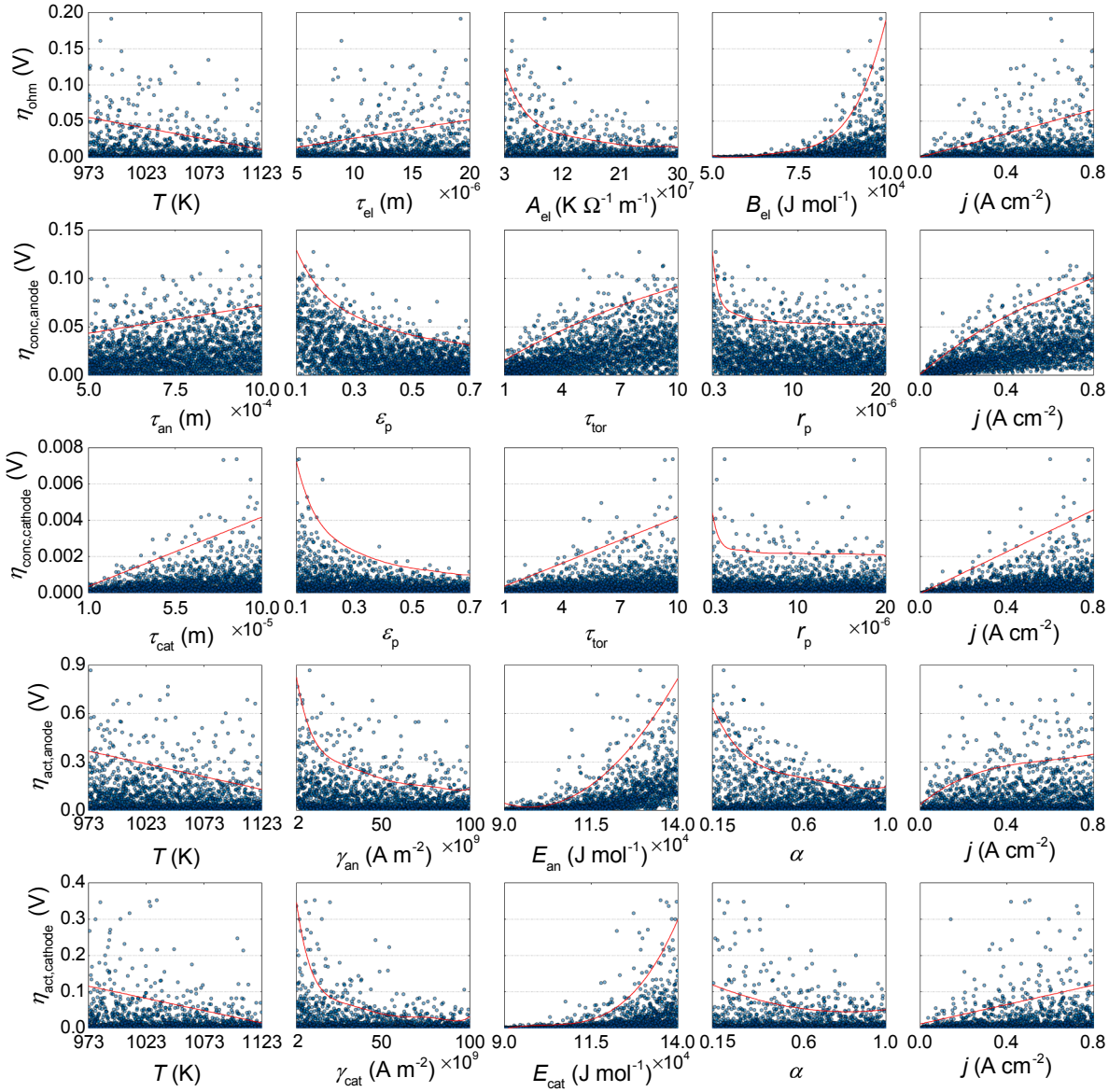

Fig. 5. Marginal effect of sensitive parameters on Ohmic, concentration, and activation overpotentials. The blues dots represent the values of overpotentials with respect to different uncertain parameters. The red lines show the evolution of overpotentials with respect to a single parameter averaged on other parameters. Note these lines are scaled for ease of view.

concentration overpotential of the anode-supported SOFC, it is important to optimize the microstructure of the anode.

Activation overpotential – Typically, the activation overpotential affects the electrochemical performance of SOFC drastically. As shown in Fig. 3, at the present condition considered in this work, the maximum value of anodic activation overpotential is larger than 0.9 V, and that of cathodic activation overpotential reaches about 0.6 V, which are apparently larger than that of the Ohmic and concentration overpotentials. Activation overpotential is potentially influenced by many parameters, e.g., temperature, porosity of electrodes, electronic transfer coefficient, and activation energy. In Fig. 4, we observe that the reaction kinetic parameters, i.e., activation energy E_{an} and E_{cat}, and pre-exponential coefficients γ_{an} and γ_{cat}, are the most important parameters, contributing more than 40% to the variance of the activation overpotential. Conversely, parameters including porosity, tortuosity, and thickness of electrodes show very small Sobol' indices (less than 0.02, not shown in the figure), indicating that they have little influence on the activation overpotential, which also implies the reaction kinetics of the considered SOFC unit is only slightly affected by the reactant and product concentrations at TPBs.

The marginal effect of the sensitive parameters plotted in Fig. 5 shows that the activation overpotential decreases with the increase of pre-exponential coefficients. A significant drop can be found in both $\eta_{act,anode}$ and $\eta_{act,cathode}$ when the pre-exponential coefficients increase from 2×10^9 A m^{-2} to about 20×10^9 A m^{-2}. Contrarily, the increase of activation energy enhances $\eta_{act,anode}$ and $\eta_{act,cathode}$ exponentially, owing to the fact that the increase of activation energy enlarges the size of the energy barrier between the reactant and activated states, which affects the reaction kinetics adversely. Specifically, to lower the activation overpotential, the univariate effect of E_{an} and E_{cat} suggests a desired activation energy in both the anode and cathode layers to be less than 11×10^4 J mol^{-1}. Besides, increasing the electronic transfer coefficient α can lead to a lower activation overpotential as well. But the effect of α is not as significant as that of E_{an}, E_{cat}, γ_{an}, and γ_{cat}.

The differences between total and first-order Sobol' indices imply the important interactive effect of parameters on activation overpotential. It is shown in Fig. 6 that the activation energy, pre-exponential coefficient, and electronic transfer coefficient not only exhibit

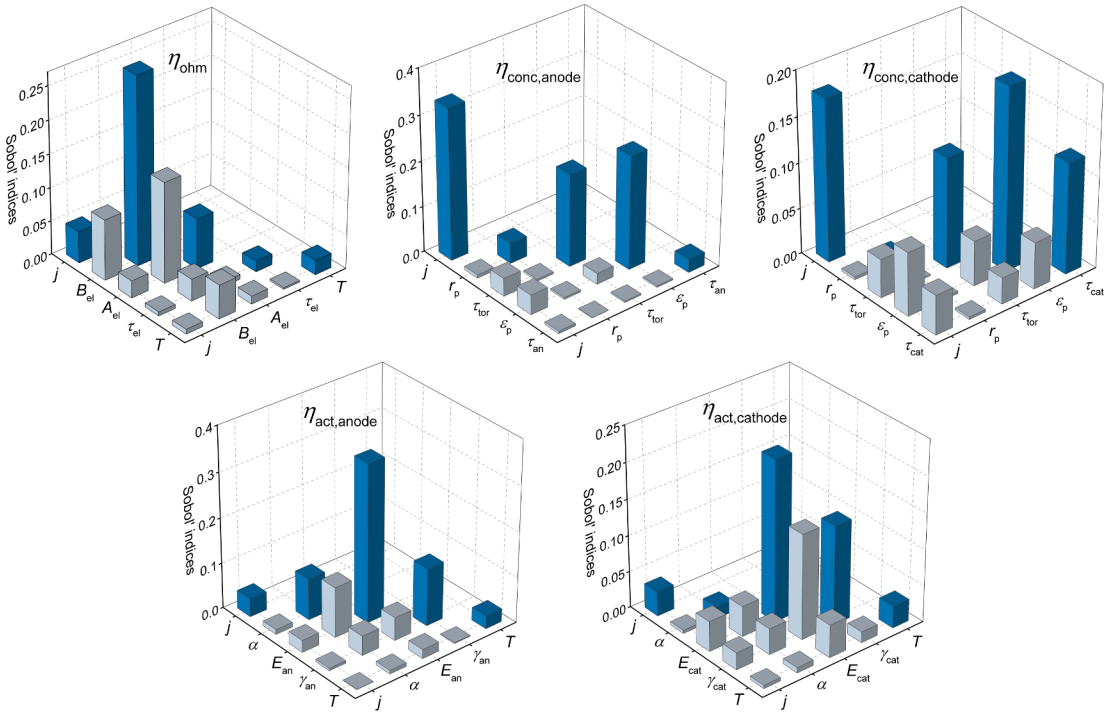

Fig. 6. Second-order Sobol' indices of sensitive parameters for Ohmic, concentration, and activation overpotentials. On the diagonal, the blue bars represent the values of first-order sensitivity indices of parameters, while the quantified pairwise interactions between every two parameters are depicted in the off-diagonal grey bars.

high univariate effects on activation overpotential, but also contribute a considerable pairwise interaction effect, which emphasizes the importance of these parameters to the optimal design of SOFCs. Essentially, the selection of the catalyst on the surface of electrodes determines the values of E_{an}, E_{cat}, and α. For instance, a catalytic electrode lowers the activation barrier for the reaction by changing the free-energy surface, which consequently decreases the activation energy and reduces the activation overpotential. In fact, a highly catalytic electrode with large electronic transfer coefficient provides the possibility of lowering the activation overpotential significantly. Therefore, the choice of catalyst in SOFCs is rather important to reduce the activation overpotential. Besides, the measurement and identification of the corresponding reaction kinetic parameters in SOFCs are essential for the accurate prediction of the activation overpotential.

5.2. GSA of the output voltage

GSA of the output voltage of a SOFC is a complex task, as the Ohmic, concentration, and activation overpotentials are considered, and all the 19 uncertain input parameters are expected to affect the output voltage prediction. According to the computed first-order and total Sobol' indices, 10 parameters that have major contributions to the variance of output voltage are listed in Fig. 7(a). Apparently, the activation energy E_{an}, pre-exponential coefficient γ_{an} of anode, and current density j are the most influential parameters, with the values of their first-order Sobol' indices being larger than 0.1, and explaining about 50% of the total variance of output voltage. Besides, large differences are observed between the total and first-order Sobol' indices for E_{an}, γ_{an}, and α. Checking the second-order Sobol' indices plotted in Fig. 7(b) indicates that these three parameters provide the most significant pairwise interaction effect. The marginal effect shown in Fig. 7(c) generally agrees with the values of Sobol' indices. It is noted that the increase of pre-exponential coefficients γ_{an} and γ_{cat}, electronic coefficient α, or the decrease of activation energy E_{an} and E_{cat}, that significantly reduce the activation overpotentials as stated before, in turn lead to a considerable rise of the output voltage. Meanwhile, the A_{el} and B_{el} that mainly affect the Ohmic overpotential are found to have a little contribution on the variance of the output voltage. This is due to the fact that the variations of anodic and cathodic activation overpotentials are relatively significant comparing to the Ohmic and concentration overpotentials for the cases studied in this work. Thus, the variance of the output voltage is mainly attributed to the parameters that are important for activation overpotentials. Moreover, the high current density enhances all the overpotentials, eventually resulting in a low output voltage. In contrast, high temperature reduces the Ohmic and activation overpotentials, and thus increases the output voltage considerably.

Examining the 19 input parameters, we find that the thickness of electrodes and electrolyte, the electronic conductivity coefficients, the tortuosity, and the average pore radius of the anode and cathode have little impact on the output voltage of the studied anode-supported SOFC. While the operating conditions, e.g., the operating temperature and the current density, are important to the SOFC output voltage. The most influential factors are the reaction kinetic parameters of the electrodes, i.e., γ_{an}, γ_{cat}, E_{an}, E_{cat}, and α, which are related to the selection of catalysts for electrochemical reactions. The porosity of electrodes slightly affects the output voltage due to the low concentration overpotential obtained in this study. This is probably because the interval of current density considered in this work is still far from the limiting current density, thus mass transport limitations are not significant. The ionic conductivity coefficients of the electrolyte, which determine the ionic conductivity and Ohmic overpotential of the SOFC, do not play a very important role in the total variance of the output voltage as expected, because the electrolyte thickness is rather small in the considered anode-supported SOFC. Thus, to improve the electrochemical performance of SOFC and to obtain the desired power density, it is important to optimize the process of electrochemical reaction kinetics, including the selection of appropriate catalysts and understanding of reaction mechanisms. Besides, the interaction effects between parameters indicate that optimizing the interactive parameters simultaneously is more efficient and effective in the optimal design of SOFCs. Furthermore, to precisely predict the electrochemical performance of the SOFC with the current model, the measurement and

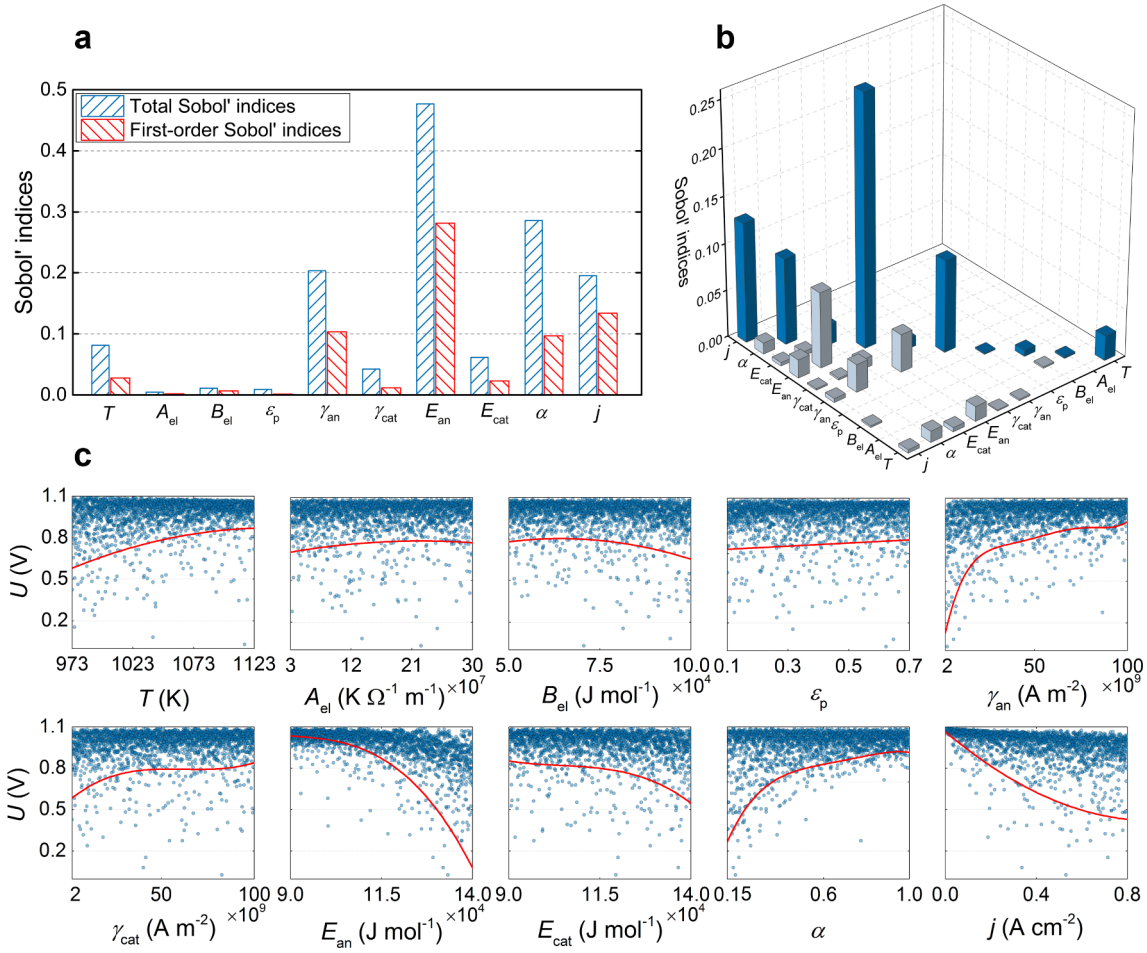

Fig. 7. Results of GSA on the output voltage of SOFCs. (a) First-order and total Sobol' indices of 10 of the most sensitive parameters for the output voltage. (b) Second-order Sobol' indices of these sensitive parameters for the output voltage. (c) Marginal effect of sensitive parameters on the output voltage. Note that the red lines representing the univariate effect of parameters are scaled for ease of view.

identification of the electrochemical reaction kinetic parameters are particularly essential.

6. Conclusions

In this work, the impact of 19 input parameters related to the microstructure of the electrodes, material properties, cell structural geometries, electrochemical reaction kinetics, and operating conditions on the solid oxide fuel cell performance are investigated by performing global sensitivity analysis on the electrochemical model of a fuel cell. To compute the sensitivity indices efficiently, the Bayesian sparse polynomial chaos expansion approach is adopted by constructing a machine-learning model for each model output with a training data set of size 2^{11}. The constructed machine-learning models are validated to ensure they are sufficiently accurate to obtain reliable sensitivity indices. Moreover, although not investigated in the present work, the machine-learning models can be used as efficient alternatives to the original electrochemical model to predict cell performance in the case where an extremely large number of simulations are needed. This as well uncovers the possibility to apply data science techniques to the field of fuel cell technologies.

Using the Bayesian sparse polynomial chaos expansion models, the individual effect of each parameter and its interactions with other parameters on the Ohmic, concentration, and activation overpotentials as well as the output voltage for an anode-supported solid oxide fuel cell are quantitatively assessed with the first-order and total Sobol' indices. In particular, the pairwise interactions between important parameters are gauged by second-order Sobol' indices. The marginal effect of each parameter is depicted to examine how the cell performance varies with the change of each parameter, which allows one to tailor the critical region of the input parameters. The results reveal that for the anode-supported fuel cell, although the thickness of the electrolyte is relatively small, the Ohmic overpotential is dominated by the ionic conductivity of electrolyte, indicating the importance of precise measurement of the ionic conductivity and appropriate choice of electrolyte materials. The concentration overpotential is influenced by the thickness and microstructural properties of electrodes, an optimal design of which is expected to reduce the voltage losses due to species concentrations. The activation overpotential plays the most important role in the voltage losses as compared to the Ohmic and concentration overpotentials. Thus, critical parameters such as the pre-exponential coefficients, the activation energy, and the electronic transfer coefficient that have significant impact on the activation overpotentials also show major influence on the cell output voltage, both individually and interactively. Therefore, to predict the cell output voltage accurately and to improve cell performance, electrochemical reaction kinetics of solid oxide fuel cells and the associated parameters are subjected to further in-depth investigations.

This work shows the effectiveness of the Bayesian sparse polynomial chaos expansion approach for performing global sensitivity analysis on the electrochemical model of solid oxide fuel cells. Insightful information about the input-output relationship of the model is uncovered via

sensitivity analysis. The results of this study are expected to provide a fundamental guideline for the design, optimization, fabrication, as well as application, of solid oxide fuel cells.

Declaration of Competing Interest

The authors declare that they have no known competing financial interests or personal relationships that could have appeared to influence the work reported in this paper.

Acknowledgments

This work has been supported by the National Natural Science Foundation of China (Grant No.: 11702199 and 11902225), and the Natural Science Foundation of Hubei Province (Grant No.: 2017CFB147).

Appendix A. Supplementary material

Supplementary data associated with this article can be found, in the online version, at https://doi.org/10.1016/j.apenergy.2019.114318.

References

[1] Gholaminezhad I, Jafarpur K, Paydar MH, Karimi G. Multi-scale multi-objective optimization and uncertainty analysis of methane-fed solid oxide fuel cells using monte carlo simulations. Energy Convers Manage 2017;153:175–87. https://doi.org/10.1016/j.enconman.2017.10.011.

[2] Li A, Song C, Lin Z. A multiphysics fully coupled modeling tool for the design and operation analysis of planar solid oxide fuel cell stacks. Appl Energy 2017;190:1234–44. https://doi.org/10.1016/J.APENERGY.2017.01.034.

[3] Choi YM, Lin MC, Liu M. Rational design of novel cathode materials in solid oxide fuel cells using first-principles simulations. J Power Sources 2010;195(5):1441–5. https://doi.org/10.1016/j.jpowsour.2009.09.017.

[4] Yan M, Zeng M, Chen Q, Wang Q. Numerical study on carbon deposition of SOFC with unsteady state variation of porosity. Appl Energy 2012;97:754–62. https://doi.org/10.1016/J.APENERGY.2012.02.055.

[5] Harun NF, Tucker D, Adams TA. Impact of fuel composition transients on SOFC performance in gas turbine hybrid systems. Appl Energy 2016;164:446–61. https://doi.org/10.1016/J.APENERGY.2015.11.031.

[6] Mahato N, Banerjee A, Gupta A, Omar S, Balani K. Progress in material selection for solid oxide fuel cell technology: a review. Prog Mater Sci 2015;72:141–337. https://doi.org/10.1016/j.pmatsci.2015.01.001.

[7] Shao Q, Bouhala L, Fiorelli D, Fahs M, Younes A, Núñez P, et al. Influence of fluid flow and heat transfer on crack propagation in SOFC multi-layered like material with anisotropic porous layers. Int J Solids Struct 2016;78–79:189–98. https://doi.org/10.1016/j.ijsolstr.2015.08.026.

[8] Al-Masri A, Peksen M, Blum L, Stolten D. A 3D CFD model for predicting the temperature distribution in a full scale APU SOFC short stack under transient operating conditions. Appl Energy 2014;135:539–47. https://doi.org/10.1016/J.APENERGY.2014.08.052.

[9] Fang X, Lin Z. Numerical study on the mechanical stress and mechanical failure of planar solid oxide fuel cell. Appl Energy 2018;229:63–8. https://doi.org/10.1016/J.APENERGY.2018.07.077.

[10] Menon V, Banerjee A, Dailly J, Deutschmann O. Numerical analysis of mass and heat transport in proton-conducting SOFCs with direct internal reforming. Appl Energy 2015;149:161–75. https://doi.org/10.1016/J.APENERGY.2015.03.037.

[11] Fardadi M, McLarty DF, Jabbari F. Investigation of thermal control for different SOFC flow geometries. Appl Energy 2016;178:43–55. https://doi.org/10.1016/J.APENERGY.2016.06.015.

[12] Bhattacharyya D, Rengaswamy R. Transport, sensitivity, and dimensional optimization studies of a tubular Solid Oxide Fuel Cell. J Power Sources 2009;190(2):499–510. https://doi.org/10.1016/J.JPOWSOUR.2008.12.084.

[13] Shao Q, Fernández-González R, Mikdam A, Bouhala L, Younes A, Núñez P, et al. Influence of heat transfer and fluid flow on crack growth in multilayered porous/dense materials using XFEM: Application to Solid Oxide Fuel Cell like material design. Int J Solids Struct 2014;51(21–22):3557–69. https://doi.org/10.1016/j.ijsolstr.2014.06.011.

[14] Zhu J, Lin Z. Degradations of the electrochemical performance of solid oxide fuel cell induced by material microstructure evolutions. Appl Energy 2018;231:22–8. https://doi.org/10.1016/J.APENERGY.2018.09.127.

[15] Zhang W, Cho C, Piao C, Choi H. Sobol's sensitivity analysis for a fuel cell stack assembly model with the aid of structure-selection techniques. J Power Sources 2016;301:1–10. https://doi.org/10.1016/J.JPOWSOUR.2015.08.076.

[16] Saltelli A, Ratto M, Andres T, Campolongo F, Cariboni J, Gatelli D, et al. Global sensitivity analysis: the primer. Chichester: John Wiley and Sons; 2008. https://doi.org/10.1111/j.1751-5823.2008.00062_17.x.

[17] Chan S, Khor K, Xia Z. A complete polarization model of a solid oxide fuel cell and its sensitivity to the change of cell component thickness. J Power Sources 2001;93(1–2):130–40. https://doi.org/10.1016/S0378-7753(00)00556-5.

[18] Campanari S, Iora P. Definition and sensitivity analysis of a finite volume SOFC model for a tubular cell geometry. J Power Sources 2004;132(1–2):113–26. https://doi.org/10.1016/j.jpowsour.2004.01.043.

[19] Nagel FP, Schildhauer TJ, Biollaz SM, Stucki S. Charge, mass and heat transfer interactions in solid oxide fuel cells operated with different fuel gases—a sensitivity analysis. J Power Sources 2008;184(1):129–42. https://doi.org/10.1016/J.JPOWSOUR.2008.05.044.

[20] Nam JH. A sensitivity map for the dependence of current generation performance on electrode microstructural parameters in solid oxide fuel cells: effectiveness model predictions. Electrochim Acta 2016;221:8–13. https://doi.org/10.1016/j.electacta.2016.10.145.

[21] Gazzarri J, Kesler O. Short stack modeling of degradation in solid oxide fuel cells: Part II. Sensitivity and interaction analysis. J Power Sources 2008;176(1):155–66. https://doi.org/10.1016/J.JPOWSOUR.2007.10.046.

[22] Göll S, Samsun R, Peters R. Analysis and optimization of solid oxide fuel cell-based auxiliary power units using a generic zero-dimensional fuel cell model. J Power Sources 2011;196(22):9500–9. https://doi.org/10.1016/J.JPOWSOUR.2011.07.030.

[23] Dhingra H, Peppley BA. Sensitivity analysis of a 1 kW diesel-fuelled SOFC generator: a single and paired-variable study. J Power Sources 2013;239:527–37. https://doi.org/10.1016/J.JPOWSOUR.2013.03.107.

[24] Cornu TM, Wuillemin Z. Impact of random geometric distortions on the performance and reliability of an SOFC. Fuel Cells 2011;11(4):553–64. https://doi.org/10.1002/fuce.201000120.

[25] He Z, Li H, Birgersson E. Correlating variability of modeling parameters with non-isothermal stack performance: Monte Carlo simulation of a portable 3D planar solid oxide fuel cell stack. Appl Energy 2014;136:560–75. https://doi.org/10.1016/J.APENERGY.2014.09.056.

[26] Kapadia S, Anderson W. Sensitivity analysis for solid oxide fuel cells using a three-dimensional numerical model. J Power Sources 2009;189(2):1074–82. https://doi.org/10.1016/J.JPOWSOUR.2008.12.130.

[27] Pan W, Bao J, Lo C, Lai K, Agarwal K, Koeppel BJ, et al. A general approach to develop reduced order models for simulation of solid oxide fuel cell stacks. J Power Sources 2013;232:139–51. https://doi.org/10.1016/J.JPOWSOUR.2013.01.057.

[28] Ferretti F, Saltelli A, Tarantola S. Trends in sensitivity analysis practice in the last decade. Sci Total Environ 2016;568:666–70. https://doi.org/10.1016/J.SCITOTENV.2016.02.133.

[29] Song X, Zhang J, Zhan C, Xuan Y, Ye M, Xu C. Global sensitivity analysis in hydrological modeling: review of concepts, methods, theoretical framework, and applications. J Hydrol 2015;523:739–57. https://doi.org/10.1016/J.JHYDROL.2015.02.013.

[30] Sobol' IM. Sensitivity estimates for nonlinear mathematical models. Math Model Comput Exp 1993;1(4):407–14. doi:1061-7590/93/04407-008.

[31] Oakley JE, O'Hagan A. Probabilistic sensitivity analysis of complex models: a Bayesian approach. J Roy Stat Soc Ser B: Stat Methodol 2004;66(3):751–69. https://doi.org/10.1111/j.1467-9868.2004.05304.x.

[32] Sudret B. Global sensitivity analysis using polynomial chaos expansions. Reliab Eng Syst Saf 2008;93(7):964–79. https://doi.org/10.1016/j.ress.2007.04.002.

[33] Blatman G, Sudret B. An adaptive algorithm to build up sparse polynomial chaos expansions for stochastic finite element analysis. Probab Eng Mech 2010;25(2):183–97. https://doi.org/10.1016/J.PROBENGMECH.2009.10.003.

[34] Blatman G, Sudret B. Adaptive sparse polynomial chaos expansion based on least angle regression. J Comput Phys 2011;230(6):2345–67. https://doi.org/10.1016/J.JCP.2010.12.021.

[35] Hu C, Youn BD. Adaptive-sparse polynomial chaos expansion for reliability analysis and design of complex engineering systems. Struct Multidiscipl Optimiz 2011;43(3):419–42. https://doi.org/10.1007/s00158-010-0568-9.

[36] Shao Q, Younes A, Fahs M, Mara TA. Bayesian sparse polynomial chaos expansion for global sensitivity analysis. Comput Methods Appl Mech Eng 2017;318:474–96. https://doi.org/10.1016/j.cma.2017.01.033.

[37] Shao Q, Liu J, Huang Q, Yang J, Hu H, Belouettar S, et al. A data-driven analysis on bridging techniques for heterogeneous materials and structures. Mech Adv Mater Struct 2019:1–15. https://doi.org/10.1080/15376494.2018.1546415.

[38] Aguiar P, Adjiman CS, Brandon NP. Anode-supported intermediate temperature direct internal reforming solid oxide fuel cell. I: model-based steady-state performance. J Power Sources 2004;138(1–2):120–36. https://doi.org/10.1016/j.jpowsour.2004.06.040.

[39] Lu N, Li Q, Sun X, Khaleel MA. The modeling of a standalone solid-oxide fuel cell auxiliary power unit. J Power Sources 2006;161(2):938–48. https://doi.org/10.1016/j.jpowsour.2006.05.009.

[40] Yang T, Liu J, Finklea H, Abernathy HW, Hackett GA. Multi-physics simulation of SOFC button cell with multi-step charge transfer model in composite LSM/YSZ cathode. ECS Trans 2017;78(1):2699–709. https://doi.org/10.1149/07801.2699ecst.

[41] Arpino F, Carotenuto A, Massarotti N, Nithiarasu P. A robust model and numerical approach for solving solid oxide fuel cell (SOFC) problems. Int J Numer Meth Heat Fluid Flow 2008;18(7–8):811–34. https://doi.org/10.1108/09615530810898971.

[42] Shao Q, Fernández-González R, Ruiz-Morales JC, Bouhala L, Fiorelli D, Younes A, et al. An advanced numerical model for energy conversion and crack growth predictions in Solid Oxide Fuel Cell units. Int J Hydrogen Energy 2015;40(46):16509–20. https://doi.org/10.1016/j.ijhydene.2015.10.016.

[43] O'Hayre R, Cha S-W, Colella WG, Prinz FB. Fuel cell fundamentals. Hoboken, New Jersey: John Wiley and Sons; 2016. https://doi.org/10.1002/9781119191766.

[44] Tseronis K, Bonis I, Kookos IK, Theodoropoulos C. Parametric and transient analysis

of non-isothermal, planar solid oxide fuel cells. Int J Hydrogen Energy 2012;37(1):530–47. https://doi.org/10.1016/j.ijhydene.2011.09.062.
[45] Huang H, Lin J, Wang Y, Wang S, Xia C, Chen C. Facile one-step forming of NiO and yttrium-stabilized zirconia composite anodes with straight open pores for planar solid oxide fuel cell using phase-inversion tape casting method. J Power Sources 2015;274:1114–7. https://doi.org/10.1016/j.jpowsour.2014.10.190.
[46] Chen D, Lin Z, Zhu H, Kee RJ. Percolation theory to predict effective properties of solid oxide fuel-cell composite electrodes. J Power Sources 2009;191(2):240–52. https://doi.org/10.1016/j.jpowsour.2009.02.051.
[47] Shi Y, Cai N, Li C, Bao C, Croiset E, Qian J, et al. Modeling of an anode-supported Ni-YSZ|Ni-ScSZ|ScSZ|LSM-ScSZ multiple layers SOFC cell. Part I. Experiments, model development and validation. J Power Sources 2007;172(1):235–45. https://doi.org/10.1016/j.jpowsour.2007.04.037.
[48] Ding J, Liu J. An anode-supported solid oxide fuel cell with spray-coated yttria-stabilized zirconia (YSZ) electrolyte film. Solid State Ionics 2008;179(21–26):1246–9. https://doi.org/10.1016/j.ssi.2008.01.094.
[49] Anselmi-Tamburini U, Chiodelli G, Arimondi M, Maglia F, Spinolo G, Munir ZA. Electrical properties of Ni/YSZ cermets obtained through combustion synthesis. Solid State Ionics 1998;110(1–2):35–43. https://doi.org/10.1016/s0167-2738(98)00115-5.

Supplemental Material

Global sensitivity analysis of solid oxide fuel cells with Bayesian sparse polynomial chaos expansions

Qian Shao[a,*], Enlai Gao[a], Thierry Mara[b,c], Heng Hu[a], Tong Liu[d], Ahmed Makradi[e]

[a]School of Civil Engineering, Wuhan University, 8 South Road of East Lake, Wuchang, 430072 Wuhan, PR China

[b]PIMENT, EA 4518, Université de La Réunion, FST, 15 Avenue René Cassin, 97715 Saint-Denis, Réunion

[c]European Commission, Joint Research Centre, Directorate for Foresight, Modelling, Behavioural Insights and Design for Policy, 21027 Ispra (VA), Italy

[d]School of Power and Mechanical Engineering, Wuhan University, 8 South Road of East Lake, Wuchang, 430072 Wuhan, PR China

[e]Luxembourg Institute of Science and Technology, Esch-sur-Alzette, Luxembourg

S1 Computation of effective conductivity in porous electrodes

The effective electronic conductivity through the electrode can be separated into intra-particle and inter-particle conductivities, in which the resistance caused by the inter-particle is usually negligible small [1]. Thus the effective conductivity of electrode, $\sigma_{\text{electrode,eff}}$, is estimated as

$$\sigma_{\text{electrode,eff}} = \xi_{\text{electrode}} \sigma_{\text{electrode}} \tag{S1}$$

where $\sigma_{\text{electrode}}$ is the intrinsic material conductivity and $\xi_{\text{electrode}}$ is the reduction factor which is primarily determined by the effective relative density of electrode particles. For Ni/YSZ anode and LSM/YSZ cathode, the reduction factors are estimated as follows:

$$\xi_{\text{anode}} = \left[(1 - \varepsilon_p)\, \psi_{\text{Ni}} \mathcal{P}_{\text{anode}} \right]^{\mu} \tag{S2}$$

$$\xi_{\text{cathode}} = \left[(1 - \varepsilon_p)\, \psi_{\text{LSM}} \mathcal{P}_{\text{cathode}} \right]^{\mu} \tag{S3}$$

where μ is the Bruggeman factor that considers the tortuous nature of porous electrodes, ψ_k is the volume fraction of k-particles relative to the total solids. The percolation probabilities $\mathcal{P}_{\text{anode}}$ and $\mathcal{P}_{\text{cathode}}$ are estimated as

$$\mathcal{P}_{\text{anode}} = \left[1 - \left(\frac{3.764 - Z_{\text{Ni}}}{2} \right)^{2.5} \right]^{0.4} \tag{S4}$$

*Corresponding author. E-mail address: qian.shao@whu.edu.cn.

$$\mathcal{P}_{\text{cathode}} = \left[1 - \left(\frac{3.764 - Z_{\text{LSM}}}{2}\right)^{2.5}\right]^{0.4} \tag{S5}$$

where Z_{k} is the average coordination number for electrode particles that is a function of the volume fraction and particle-radii

$$Z_{\text{Ni}} = \bar{Z}\frac{\psi_{\text{Ni}}/r_{\text{Ni}}}{\psi_{\text{Ni}}/r_{\text{Ni}} + \psi_{\text{YSZ}}/r_{\text{YSZ}}} \tag{S6}$$

$$Z_{\text{LSM}} = \bar{Z}\frac{\psi_{\text{LSM}}/r_{\text{LSM}}}{\psi_{\text{LSM}}/r_{\text{LSM}} + \psi_{\text{YSZ}}/r_{\text{YSZ}}} \tag{S7}$$

Here, $\bar{Z}$ is an overall average coordination number of all solid particles, which is widely assumed that $\bar{Z} = 6$.

S2 Validation of the electrochemical model

To justify the generality of this electrochemical model, a validation on the experimental data from Ding et al. [2] is performed. In [2], a single fuel cell of Ni-YSZ/YSZ/LSM-YSZ is tested at different operating temperatures. The anode substrate of this SOFC is prepared with a mix of NiO (synthesized by glycine-nitrate process) and YSZ (TZ-8Y, Building Material Academy of China) in a weight ratio of 1:1. The size of the anode layer is 13 mm in diameter and 0.5 mm in thickness. The YSZ film is about 15 μm. The cathode is made of a mix of LSM and YSZ in a weight ratio of 6:4. The manufactured single cell is supplied with pure, humidified ($\sim$3% H_2O) hydrogen as fuel in the anode, and stationary air as the oxidant in the cathode. The electrochemical performance of the cell is measured under open circuit condition using CHI604B (Shanghai Chenhua Instruments Ltd., China). The operating conditions and model parameters for this SOFC are listed in Table S1. Using these parameters, the output voltage and power density of the SOFC are computed at different operating temperatures based on the electrochemical model. As depicted in Fig. S1, the model-predicted results are compared with the experimental data reported in [2], where fairly good agreement is found, indicating the validity and generality of the presented mathematical model in predicting the electrochemical performance of SOFCs.

S3 GSA of power density and voltage efficiency

Except for the overpotentials and cell output voltage, the power density (P) as well as the voltage efficiency of the fuel cell ($\varepsilon_{\text{voltage}}$) are assessed to quantify the electrochemical performance

Table S1: Parameters used for SOFC electrochemical model verification

Operating temperature	$T = 1023 - 1073$ K [2]
Operating pressure	$p_0 = 1.0$ atm [2]
Fuel composition	$x_{H_2} : x_{H_2O} = 0.97 : 0.03$ [2]
Air composition	$x_{O_2} : x_{N_2} = 0.21 : 0.79$ [2]
Anode thickness	$\tau_{an} = 500.0\ \mu$m [2]
Cathode thickness	$\tau_{cat} = 20.0\ \mu$m [2]
Electrolyte thickness	$\tau_{el} = 15.0\ \mu$m [2]
Electronic conductivity of Ni	$\sigma_{Ni} = 3.27 \times 10^6 - 1065.3T\ \Omega^{-1}\ \text{m}^{-1}$ [3]
Electronic conductivity of LSM	$\sigma_{LSM} = \frac{4.2 \times 10^7}{T} \exp\left(\frac{-1150}{T}\right)\ \Omega^{-1}\ \text{m}^{-1}$ [3]
Electrolyte ionic conductivity	$\sigma_{YSZ} = 3.34 \times 10^4 \exp\left(\frac{-10300}{T}\right)\ \Omega^{-1}\ \text{m}^{-1}$ [3]
Porosity of electrodes	$\varepsilon_p = 0.3$ [4]
Tortuosity of porous electrodes	$\tau_{tor} = 8.0$ [4]
Average pore radius	$r_p = 0.8\ \mu$m [4]
Anode pre-exponential coefficient	$\gamma_{an} = 3.4 \times 10^9\ \text{A m}^{-2}$ [5]
Cathode pre-exponential coefficient	$\gamma_{cat} = 2.0 \times 10^9\ \text{A m}^{-2}$ [5]
Anode activation energy	$E_{an} = 9.0 \times 10^4\ \text{J mol}^{-1}$ [5]
Cathode activation energy	$E_{cat} = 1.03 \times 10^5\ \text{J mol}^{-1}$ [5]
Electronic transfer coefficient	α=0.16 [4]
Leak overpotential	$\eta_{leak} = 0.055$ V [2]

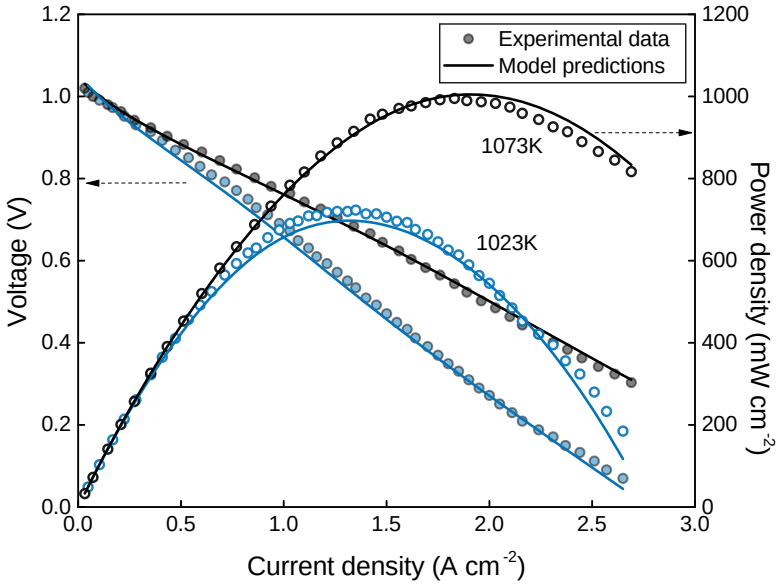

Figure S1: Comparison of the model-predicted output voltage (the descending curves) and power density (the bell-shaped curves) with the experimental data reported in [2] at different operating temperatures.

of SOFCs. The power density and voltage efficiency of the fuel cell are computed respectively by:

$$P = jU \tag{S8}$$

$$\varepsilon_{\text{voltage}} = \frac{U}{U^{\text{OCP}}} \tag{S9}$$

To perform GSA on power density and voltage efficiency, machine-learning models are constructed with BSPCE to describe the relationship between the input parameters and the output performance of SOFCs. As shown in Fig. S2, the BSPCE-predicted power density and voltage efficiency are firstly compared with the model-calculated data from the training set, and then tested by a validation set consisting of extra 2^{11} Monte Carlo simulations. The comparisons in Fig. S2 show that, for power density P, remarkable agreement is obtained between the model-calculated data and BSPCE-predicted values with the coefficients of determination (R^2) for both training and validation sets being larger than 0.99. Basically, R^2 for validation set is slightly lower than that of the training set, with a difference of around 0.003. An excellent match is found between the ideal fit and the linear fit of model-calculated data to BSPCE-predicted values, which confirms that the BSPCE models reproduce well the physical model-calculated power density. This excellent match is probably due to the fact that the power density is strongly dependent on the current density.

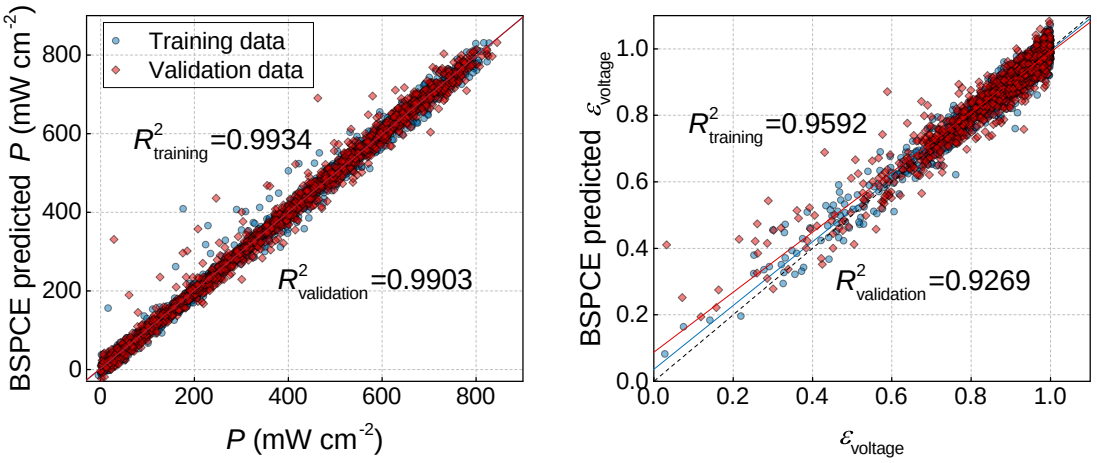

Figure S2: Comparison of model outputs (P and $\varepsilon_{\text{voltage}}$) between the BSPCE-predicted values and model-calculated data, including the training set and the validation set. The dashed lines are the ideal 1:1 ratio, whereas the solid lines are the fit to the predicted values. The deviations between the dashed lines and the solid lines show slight overestimation at low values for the voltage efficiency.

Meanwhile, for the voltage efficiency, similar as the cell output voltage, discrepancies between the BSPCE-predicted and model-calculated values are observed. Fig. S2 shows that R^2

of the voltage efficiency decreases to 0.95 and 0.92 for the training and validation set, respectively. The linear fit to the BSPCE-predicted values reveals a slight overestimation at low voltage efficiencies. The voltage efficiency is strongly dependent on the cell output voltage. Thus, the BSPCE model of voltage efficiency exhibits similar performance of that of the cell output voltage. Overall, all BSPCE models show good ability to reproduce both the training and validation sets. And the accuracy of these models is sufficient to obtain reliable sensitivity indices.

The above-presented BSPCE models are used to perform GSA on the electrochemical performance of a SOFC unit, based on which the first-order and total Sobol' indices are computed analytically for each input parameter. The Sobol' indices of the most sensitive parameters for power density are shown in Fig. S3. Apparently, the current density j is the most influential parameter, with the values of first-order Sobol' indices larger than 0.9, and explaining about 90% of the total variance of power density. The difference between the first-order and total Sobol' indices are insignificant, implying that the coupling effect between different parameters on power density is negligible. Checking the marginal effect of parameters on power density in Fig. S4 indicates that the power density increases linearly with the increase of current density. In general, further increase of current density would lower the cell output voltage, and thus lead to the decreasing of power density. This is not observed in the current study probably because the maximum current density is still far from the limiting current density.

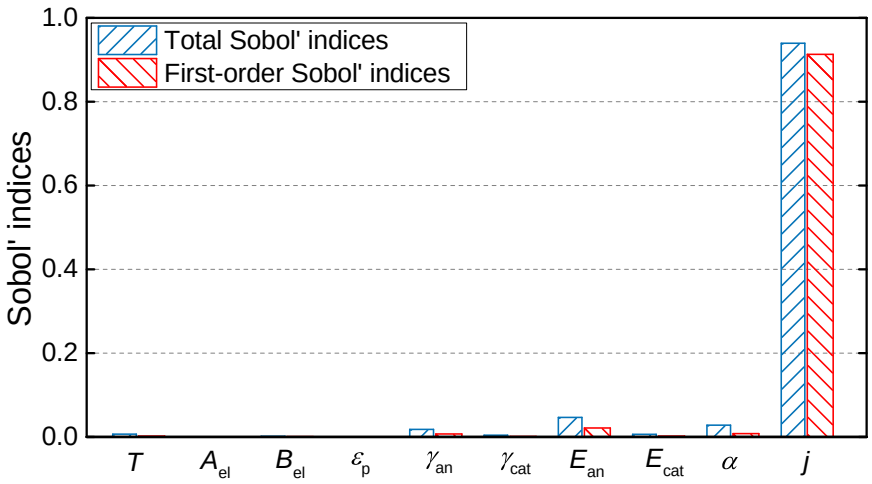

Figure S3: Total and first-order Sobol' indices of the most sensitive parameters for power density.

Voltage efficiency of SOFC is strongly dependent on the cell output voltage. According to the computed first-order and total Sobol' indices, 10 parameters that have major contributions to the variance of voltage efficiency are listed in Fig. S5. The marginal effect shown in Fig. S6

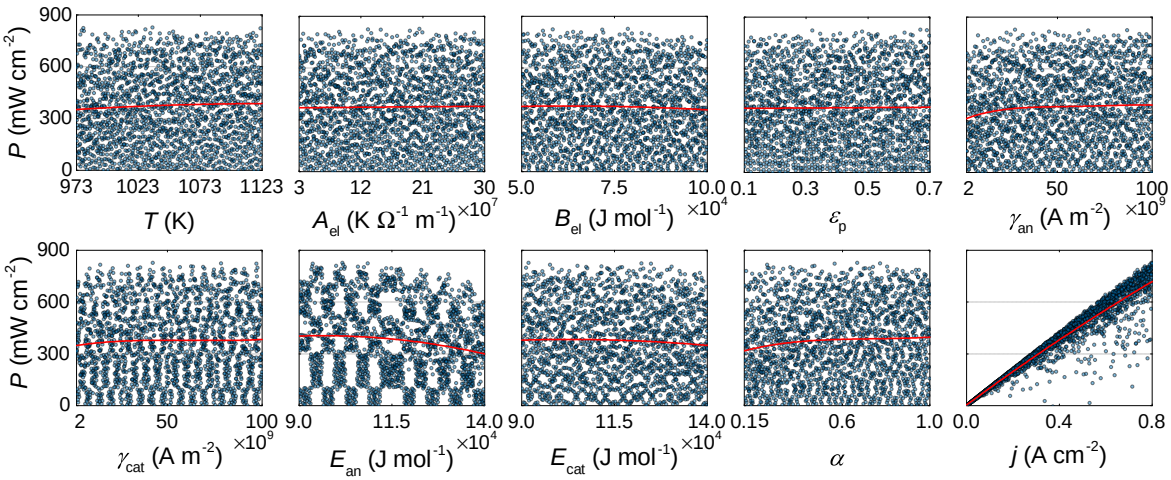

Figure S4: Marginal effect of sensitive parameters on power density. The blues dots represent the values of power density with respect to different uncertain parameters. The red lines show the evolution of power density with respect to a single parameter averaged on other parameters. Note these lines are scaled for ease of view.

generally agrees with the values of Sobol' indices. The second-order Sobol' indices are plotted in Fig. S7. It is noted that all the first-order, total Sobol' indices and marginal effects on cell efficiency show similar values and tendency as that on output voltage. And the temperature exhibits slightly more significant effect on the efficiency than on the output voltage.

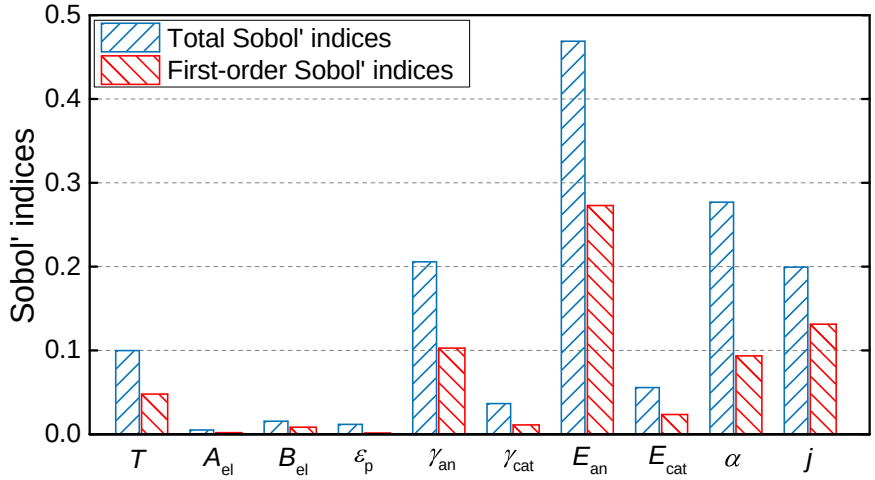

Figure S5: Total and first-order Sobol' indices of the most sensitive parameters for voltage efficiency.

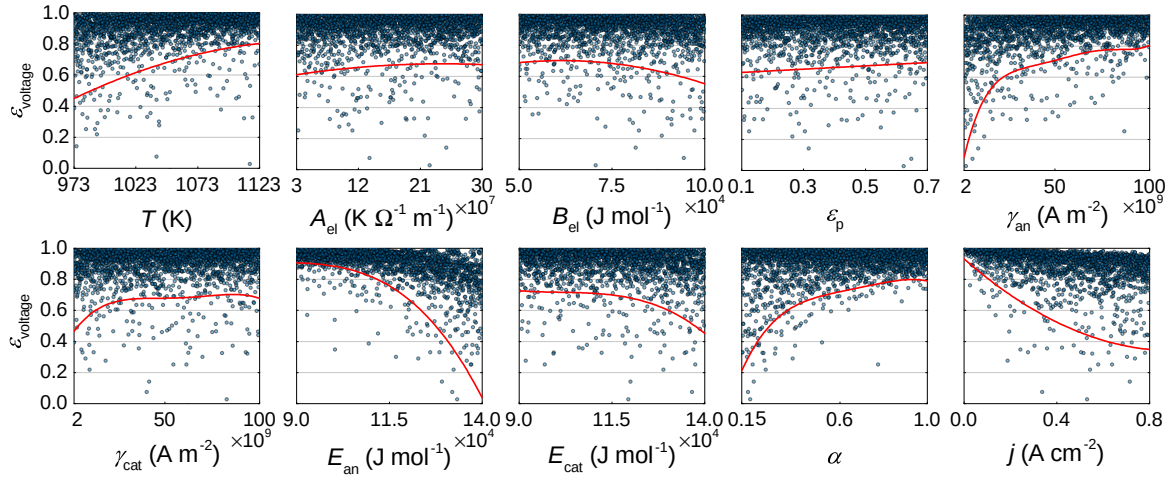

Figure S6: Marginal effect of sensitive parameters on voltage efficiency. The blues dots represent the values of efficiency with respect to different uncertain parameters. The red lines show the evolution of voltage efficiency with respect to a single parameter averaged on other parameters. Note these lines are scaled for ease of view.

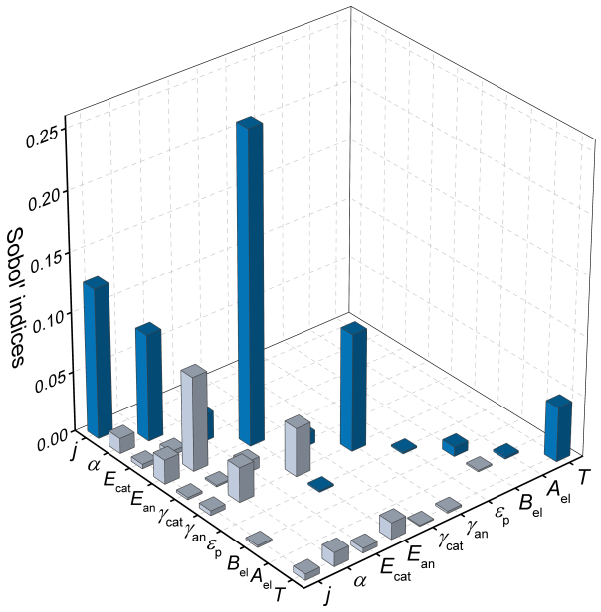

Figure S7: Second-order Sobol' indices of sensitive parameters for voltage efficiency. On the diagonal, the blue bars represent the values of first-order sensitivity indices of parameters, while the quantified pairwise interactions between every two parameters are depicted in the off-diagonal grey bars.

Acknowledgments

This work has been supported by the National Natural Science Foundation of China (Grant No.: 11702199 and 11902225), and the Natural Science Foundation of Hubei Province (Grant No.: 2017CFB147).

References

[1] D. Chen, Z. Lin, H. Zhu, R. J. Kee, Percolation theory to predict effective properties of solid oxide fuel-cell composite electrodes, Journal of Power Sources 191 (2) (2009) 240–252. doi:10.1016/j.jpowsour.2009.02.051.

[2] J. Ding, J. Liu, An anode-supported solid oxide fuel cell with spray-coated yttria-stabilized zirconia (YSZ) electrolyte film, Solid State Ionics 179 (21-26) (2008) 1246–1249. doi:10.1016/j.ssi.2008.01.094.

[3] T. Yang, J. Liu, H. Finklea, H. W. Abernathy, G. A. Hackett, Multi-physics simulation of SOFC button cell with multi-step charge transfer model in composite LSM/YSZ cathode, ECS Transactions 78 (1) (2017) 2699–2709. doi:10.1149/07801.2699ecst.

[4] R. O'Hayre, S.-W. Cha, W. G. Colella, F. B. Prinz, Fuel cell fundamentals, John Wiley and Sons, Hoboken, New Jersey, 2016. doi:10.1002/9781119191766.

[5] S. Campanari, P. Iora, Definition and sensitivity analysis of a finite volume SOFC model for a tubular cell geometry, Journal of Power Sources 132 (1-2) (2004) 113–126. doi:10.1016/j.jpowsour.2004.01.043.